Understanding ~~Absorption by Black Versus~~the Mechanism and Importance of Brown Carbon Bleaching Across the Visible Spectrum in Biomass Burning Plumes from the WE-CAN Campaign

Yingjie Shen[1], Rudra P. Pokhrel[1, *], Amy P. Sullivan[2], Ezra J. T. Levin[2, *], Lauren A. Garofalo[3], Delphine K. Farmer[3], Wade Permar[4], Lu Hu[4], Darin W. Toohey[5], Teresa Campos[6], Emily V. Fischer[2], Shane M. Murphy[1]

[1]Department of Atmospheric Science, University of Wyoming, Laramie, WY 82071, USA.
[2]Department of Atmospheric Science, Colorado State University, Fort Collins, CO 80523, USA
[3]Department of Chemistry, Colorado State University, Fort Collins, CO 80523, USA
[4]Department of Chemistry and Biochemistry, University of Montana, Missoula, MT 59812, USA.
[5]Department of Atmospheric and Oceanic Sciences, University of Colorado Boulder, Boulder, CO 80309, USA
[6]National Center for Atmospheric Research, Atmospheric Chemistry Division, Boulder, CO 80301, USA

*now at Air Pollution Control Division, Colorado Department of Public Health and Environment, Denver, CO 80246, USA

Corresponding author: Shane M. Murphy (shane.murphy@uwyo.edu)

Abstract. Aerosol absorption of visible light has an important impact on global radiative forcing. Wildfires are one of the major sources of light-absorbing aerosol, but there remains significant uncertainty about the magnitude, wavelength dependence, and bleaching of absorption from biomass burning aerosol. We collected and analyzed data from 21 Western United States wildfire smoke plumes during the 2018 WE-CAN airborne measurement campaign to determine the contribution of black carbon (BC), brown carbon (BrC), and lensing to the aerosol mass absorption cross-section (MAC). ~~MAC_{BC}, MAC of organics ($MAC_{BrC+lensing}$),~~Comparison to commonly used parameterizations and modeling studies suggest model overestimation of absorption is likely due to incorrect BrC refractive indices. Modelers (Wang et al. 2018; Carter et al. 2021) invoke a bleaching process that decreases the MAC of ~~water-soluble BrC (MAC_{ws_BrC660}) are calculated using Photoacoustic Absorption Spectrometer, Single Particle Soot Photometer and Particle into Liquid Sampler measurements. MAC_{BC660} does not change significantly with physical age,~~ organic aerosol (OA) ~~concentration,~~ to offset the overestimation of absorption in models. However, no evidence of decreasing MAC is observed in individual WE-CAN fire plumes or in aged plumes from multiple fires. A decrease in OA mass and water-soluble organic carbon (WSOC), both normalized by CO to correct for dilution, is observed with increasing oxygen to carbon (O:C) ratio ~~(O:C),~~ and decreasing gas-phase toluene:benzene ratio, ~~modified combustion efficiency (MCE), altitude, or temperature, and has a relatively stable~~when data from all fires is combined and in half of individual fire plumes. This results in a strong decrease in total absorption at 405 nm and slight decrease at 660 nm with these chemical markers. These results demonstrate that changes in absorption with chemical markers of plume age are the result of decreasing OA rather than changes in the MAC of the organic material itself. While decreasing MAC or OA mass with aging could both be called bleaching, and can both correct overestimation of absorption in models, it's important to distinguish these two effects because decreasing OA mass will also decrease scattering, which

will cause a significantly different net radiative effect. We also find that an average ~~value of 10.9 ± 2.1 $m^2 g^{-1}$. On average,~~of 54% of non-BC absorption (23% total absorption) at 660 nm is from water-soluble BrC~~. MAC_{ws_BrC660} is 0.06 ± 0.04 $m^2 g^{-1}$ while $MAC_{BrC+lensing}$ is 0.11 ± 0.06 $m^2 g^{-1}$ at 660 nm, increasing to 0.59 ± 0.19 $m^2 g^{-1}$ at 405 nm. $MAC_{BrC+lensing}$ is constant with physical age and MCE, but increases slightly with increasing O:C or decreasing toluene:benzene, while total absorption (normalized to CO) slightly decreases with increasing O:C or decreasing toluene:benzene due to decreasing OA. No evidence of~~, confirming that BrC ~~bleaching is observed. Comparison to commonly used parameterizations, modeling studies, and the FIREX-AQ observations suggest model overestimation of absorption is likely due to incorrect BrC refractive indices.~~ absorption is important across the visible spectrum. Quantification of significant ~~brown carbon~~BrC ~~in the~~at red wavelengths and the ~~stability of MAC_{BC}, the~~ observation of ~~minimal~~ bleaching~~, and the observation of~~ being caused by changes in OA with O:C and toluene:benzene markers ~~all serve as important~~of plume age provide important improvements to our understanding of BrC and critical constraints on aerosol absorption in regional and global climate models.

1 Introduction

Atmospheric aerosol impact the climate system by directly scattering and absorbing solar radiation, by indirectly changing cloud properties, and through deposition that changes the surface albedo (McConnell et al., 2007; Sarangi et al., 2020). Biomass burning injects a large amount of primary organic aerosol (POA), secondary organic aerosol (SOA) and black carbon (BC) into the atmosphere every year. BC is somewhat poorly defined, but is generally considered to be insoluble and refractory and includes a variety of materials such as char, biochar, charcoal, elemental carbon (EC), and soot (Wei et al., 2013). Although it only represents a small fraction of aerosol mass, BC has a significant impact on the global energy budget due to its ability to strongly absorb solar radiation~~.~~ at all visible wavelengths. While still important, positive radiative forcing of BC is lower in IPCC AR6 (2022) than in IPCC AR5 (2013). Bond et al. (2013) estimated the direct radiative forcing for BC from 1750 to 2005 at the top of the atmosphere (TOA) to be +0.71 W m^{-2}, with an uncertainty of 90% while the latest IPCC AR6 (2022) estimates effective radiative forcing for BC from 1750 to 2019 to be +0.11 (-0.2 ~ +0.42) W m^{-2}. It is important to note that AR5 reported direct radiative forcing while AR6 reports effective radiative forcing. While BC is emitted from nearly all combustion processes, the largest global source of BC is thought to be biomass burning (Bond et al., 2013). Organic aerosol (OA) also absorbs visible light, but its absorption strongly depends on the wavelength of light (Kirchstetter and Novakov, 2004). Non-BC light absorbing organic compounds are often called brown carbon (BrC) and they are usually co-emitted with BC or formed by secondary chemistry in biomass burning plumes (Andreae and Gelencsér, 2006). Unlike BC, which absorbs light from the UV to the IR, BrC absorption sharply increases in the UV and shorter visible portions of the spectrum and has been historically considered to be almost transparent near the red wavelengths (Andreae and Gelencsér, 2006; Bahadur et al., 2012; Liu et al., 2020). The global-mean TOA direct radiative forcing from BrC also shows a large uncertainty, with estimates ranging from +0.03 W m^{-2} to +0.57 W m^{-2} (Saleh, 2020). Wildfires in the Western U.S. have increased in recent decades (Westerling et al., 2006; Burke et al., 2021), and will continue increasing according to model predictions (Yue et al., 2013; Hurteau et al., 2014; Ford et al., 2018; Neumann et al.,

2021). Therefore, quantitative studies of the radiative effects caused by BC and BrC emitted from wildfires are crucial for a better understanding of future climate and essential to improve climate models.

The large uncertainty in the radiative forcing from BC is caused both by uncertainties in emissions and by uncertainty in properties that affect its optics, such as size distribution, morphology, refractive index, and mixing state (Bond et al., 2006; Kleinman et al., 2020; Brown et al., 2021). For wildfires, most of the aerosol mass is organic (Garofalo et al., 2019). When BC is internally mixed with OA, the BC is coated by other absorbing or non-absorbing materials that cause more photons to interact with the BC core, and therefore enhance the absorption of the BC core. This process is often called the lensing effect even though geometric lensing is not actually happening at these sizes (Fuller et al., 1999). The absorption enhancement caused by the lensing effect is defined as the ratio of the absorption cross-section of a coated BC particle to that of an equivalent uncoated BC particle (Lack and Cappa, 2010). Laboratory experiments have shown a strong absorption enhancement of BC by a factor of two or more (Schnaiter et al., 2003; Schnaiter et al., 2005; Bond and Bergstrom, 2006; Bond et al., 2006; Peng et al., 2016). ~~While~~ Observations of absorption enhancement from ambient BC vary widely in field studies due to variations in coating thickness, coating material, source type, or methodological differences, but it is often much lower than laboratory values (Liu et al., 2015, 2017; Cappa et al., 2012, 2019; Healy et al., 2015; Krasowsky et al., 2016). Cappa et al. (2019) summarized absorption enhancements observed at the red end of the visible spectrum from 10 studies including ambient measurements, source sampling, and lab experiments. The absorption enhancement reported by those measurements ranged from 1.1 to 2.8.

~~Three methods (referred to henceforth as core-shell Mie theory, thermal denuder, and mass absorption cross-section) can be used to obtain estimates of absorption enhancement. Numerical solutions to Mie theory (Bohren and Huffman, 1983) have been used to model aerosol absorption for many years and can be adapted into a core-shell model, which is a simplified version of the complex mixing states in real atmospheric particles (Chylek et al., 2019). The core-shell model assumes particles are concentric spheres, where BC acts as a core and the other materials (typically organics) act as a shell. This model can simulate the absorption enhancement with geometric and optical inputs (i.e., shell thickness, particle radius, refractive index). However, the assumptions made by Mie theory may have significant errors for irregular particles, often found in fresh soot particles and when mixed BC and organics are not concentric spheres. A thermodenuder can be used to remove volatile coating materials by heating them to a temperature from 250 – 400 °C. The ratio of the absorption coefficient measured in ambient air and measured after passing particles through the thermodenuder gives an empirical absorption enhancement. Liu et al. (2015) utilized a thermodenuder to find the average absorption enhancement at 405 nm and 781 nm to be 1.3 and 1.4, respectively, in the UK during winter. Pokhrel et al. (2017) utilized a photoacoustic absorption spectrometer (PAS) with a thermodenuder and showed that absorption enhancement determined in this manner depends on fuel type and combustion conditions, with absorption enhancements ranging from 0.92 to 1.43 at 660 nm and reaching a maximum of 5.6 at 405 nm. However, a thermodenuder cannot always remove coating materials completely and thus can lead to underestimates of absorption enhancement. The mass absorption cross section of BC (MAC_{BC}) is another way to describe the absorbing ability of BC containing particles by describing the absorption per unit mass of BC.~~The mass absorption cross section of BC (MAC_{BC}) is a different way to describe the absorbing ability of BC containing particles versus absorption enhancement. By describing the absorption per unit mass of BC, MAC_{BC} can be a fundamental input in climate models to convert

mass concentration into absorption coefficients (Cho et al., 2019). MAC_{BC} is the particulate absorption divided by the mass of the pure BC at the same wavelength. In this way, the calculated MAC_{BC} will include absorption of the BC core~~,~~ along with the absorption and absorption enhancement caused by the coating material. Unfortunately, the MAC of the overall BC particle, MAC_{BC}, in the ambient atmosphere continues to be ~~not well~~poorly understood due to ~~the~~a lack of field measurements and ~~instrumental~~ limitations~~. The~~ of filter-based instruments to measure this parameter. Processes that occur during atmospheric aging ~~processes on~~of BC ~~can~~also introduce uncertainties ~~on~~in its absorption. Bond and Bergstrom (2006) suggested a MAC_{BC} of 7.5±1.2 m^2 g^{-1} at 550 nm for fresh BC. Subramanian et al. (2010) reported a MAC_{BC} of 10.9±2.1 m^2 g^{-1} at 660 nm and 13.1 m^2 g^{-1} at 550 nm over Mexico City when using a single particle soot photometer (SP2) and the filter-based particle soot absorption photometer (PSAP) instrument during airborne measurements. Krasowsky et al. (2016) reported a MAC_{BC} enhancement of 1.03±0.05 due to the coatings on BC. Zhang et al. (2017) found a MAC_{BC} with a mean of 10 m^2 g^{-1} and a standard deviation of 4 m^2 g^{-1} at 660 nm by using both SP2 and PSAP measurements. Cho et al. (2019) summarized MAC_{BC} estimated from more than 10 studies in East and South Asia in both ambient conditions and laboratory experiments, and the values ranged from 4.6 to 11.3 m^2 g^{-1}.

The limitations of current measurement techniques bring major uncertainty into quantifying BrC absorption, because BrC is usually co-emitted with BC which makes it challenging to measure BrC absorption independently. BrC absorption can be directly measured through the solvent-extraction method (Peltier et al., 2007; Zeng et al., 2021; Sullivan et al., 2022) or a thermodenuder (Cappa et al., 2012; Liu et al., 2015; Pokhrel et al., 2017). However, the solvent-extraction method will miss BrC that's insoluble in water or organic solvents, and thermal denuders miss BrC that is not volatile at the denuder temperature. BrC absorption can also be calculated from multi-wavelength total absorption measurements, but this approach must assume the absorption Ångström exponent (AAE) for BC and assumes that BrC does not absorb at longer wavelengths, adding significant uncertainty.

To improve ~~the~~ understanding of the evolution of light-absorbing aerosol from biomass burning, smoke from 21 wildfires in the Western United States were measured near their sources and downwind onboard the NSF/NCAR C-130 aircraft during the Western Wildfire Experiment for Cloud Chemistry, Aerosol Absorption and Nitrogen (WE-CAN) campaign. This campaign represented ~~one of the first~~an airborne ~~attempts~~attempt to fully characterize Western U.S. wildfires from several different fuel types, locations, and fire stages (flaming vs. smoldering). This paper presents novel observations about the absorbing properties of the aerosol and compares these observations to modeling studies conducted with the WE-CAN data and to results from the Fire Influence on Regional to Global Environment – Air Quality (FIREX) study conducted in 2019 (Zeng et al., 2021).

2 Experimental Method

This work relies on measurements made during the WE-CAN field campaign, which sampled smoke emitted by wildfires across the Western U.S. using the NSF/NCAR C-130 research aircraft. The goal of the campaign was to make detailed observations of the physical, chemical, and optical evolution of aerosol in western wildfire smoke and its impact on climate, air quality, weather, and nutrient cycles. The WE-CAN field campaign consisted of 19 research flights that took place from Jul. 24 – Sep. 13, 2018. Data from 13 flights where all required instrumentation was

available were analyzed in this study. The flight path and dominant wildfire for each of these flights are shown in Fig. 1. The fire locations, fuel types for each fire during WE-CAN were characterized and summarized by Lindaas et al. (2021).

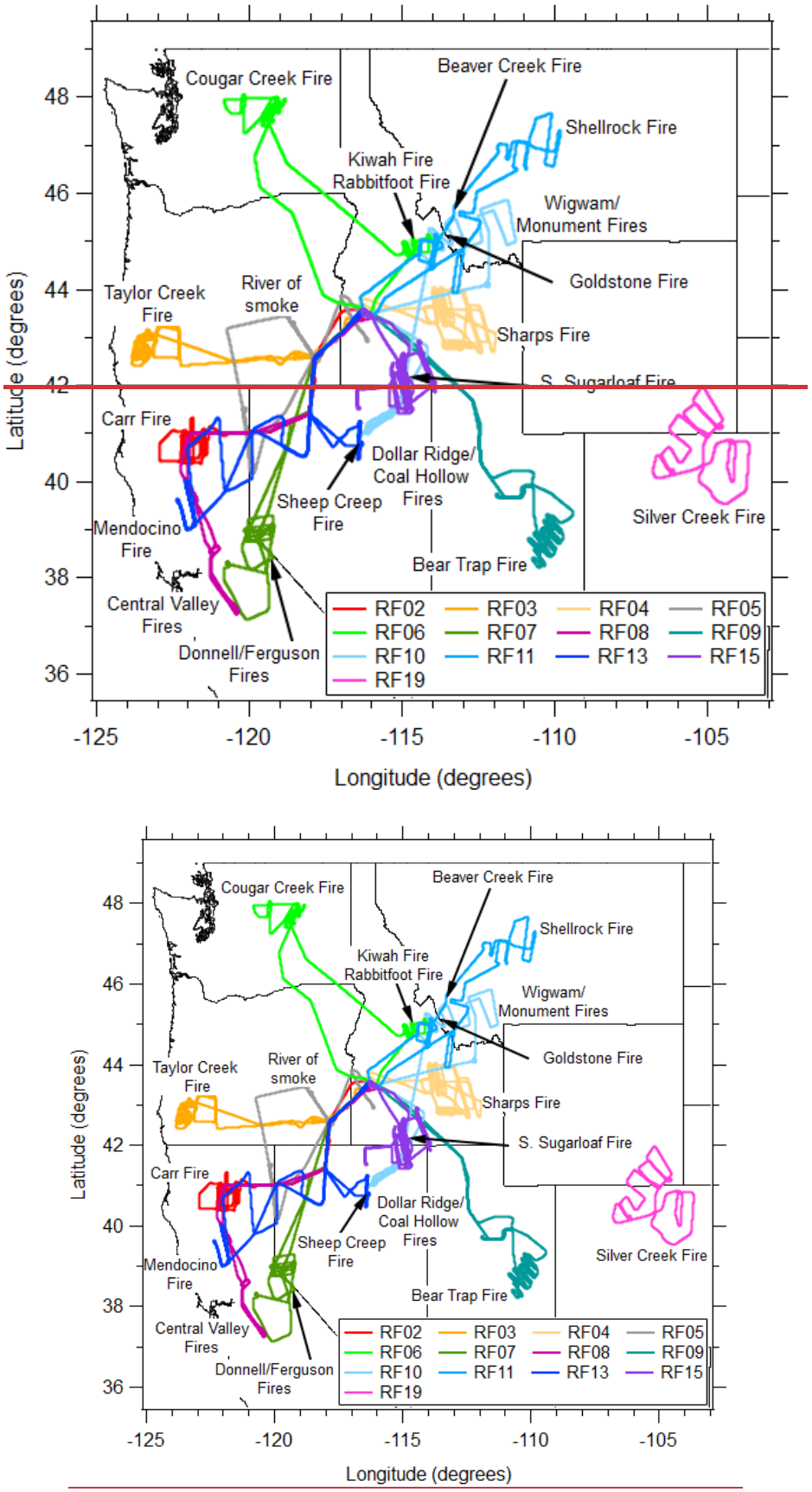

Figure 1: Flight paths and the sampled wildfires for the WE-CAN flights analyzed in this paper.

2.1 Instrumentation

The following instruments are a subset of those flown during the WE-CAN campaign and are utilized in this work. The full WE-CAN dataset is archived at https://data.eol.ucar.edu/master_lists/generated/we-can. All aerosol instruments utilized in this paper, except the PILS, ~~used~~ pulled air from the same Solid Diffuser Inlet (SDI) inlet. The PILS sampled from a Submicron Aerosol Inlet (SMAI) (Craig et al., 2013a, 2013b, 2014; Moharreri et al., 2014). All the measurements were converted to standard temperature and pressure (STP, 1 atm, 0°C) based on the measured temperature and pressure (Eq. 1) before data were uploaded.

$$Variables_{STP} = Variables_{measured} \cdot \frac{Pressure_{STP}}{Pressure_{measured}} \cdot \frac{Temperature_{measured}}{Temperature_{STP}} \quad (Eq.\,1)$$

2.1.1 Photoacoustic Absorption Spectrometer (PAS)

Aerosol absorption coefficients were measured with the multi-wavelength PAS built by the University of Wyoming (Foster et al., 2019), based on the design of Lack et al. (2012b). A PAS can directly measure the absorption coefficient of dry aerosol. The PAS represents the only way to directly measure aerosol absorption other than ~~the~~a photothermal interferometer (PTI, Sedlacek, 2007), which measures the change in the refractive index of the air near particles caused by heating from absorption. Briefly, when modulated laser light (at the resonant frequency of the cell) is absorbed by the aerosol~~,~~ it heats the surrounding air inducing pressure waves that are ~~created and~~ amplified by the cavity then detected by two microphones (Lack et al., 2006; Foster et al., 2019). The PAS used here has four cells that measure the aerosol absorption coefficient from dry air at 405 nm and 660 nm and thermally denuded air at 405 nm and 660 nm. The denuder was set to 300°C, with the goal of evaporating volatile organic aerosol which might have a potential impact on light absorption. However, absorption from the denuded channels was not used in this study, because the absorption enhancement calculated using the thermodenuder approach ~~is~~was much smaller than the approach taking the ratio of MAC_{BC} to $MAC_{BC\text{-}core}$, and we believe the discrepancy is due to the presence of significant residual organic material after denuding. Two NO_X denuders coated with potassium hydroxide, guaiacol and methanol were installed on the PAS in front of the inlet to remove the absorption from gas-phase NO_2 (Williams and Grosjean 1990). No evidence of NO_2 absorption (which would cause baseline shifts) was observed during filter measurements that are acquired every few minutes. A 3 LPM $PM_{2.5}$ cyclone (URG-2000-30ED) was used on the PAS in front of the inlet to provide a $PM_{1.0}$ cut~~,~~ under a total flow rate of 5.7 LPM. In addition, a Nafion drier (Purma Pure PD-100T-24MPS) with 100 tubes was installed on the inlet system to dry sample to a relative humidity below 30%. The particle loss (< 3%) in the drier was corrected during post-processing. The uncertainty in the absorption coefficient measured by the PAS mainly comes from the calibration technique, in which the highly absorbing substance Regal Black and the CAPS PM_{SSA} were utilized (Foster et al., 2019). The PAS was routinely calibrated (after each flight or every other day if there was a flight everyday) during WE-CAN with an accuracy of +/- 10%.

The PAS microphone shows a pressure-dependent response to pressure. To account for this behavior, we performed pressure-dependent calibration of the PAS where the instrument pressure (both PAS and CAPS PM_{SSA}) was dropped stepwise by ~50 torr from ambient to ~300 torr (typical minimum pressure level during WE-CAN). A calibration was performed at each pressure step and the calibration constants were fitted with pressure to get a change

in calibration at a desired pressure. Pressure-dependent calibrations were repeated pre and post-campaign to capture variability.

~~Aerosol optical properties (absorption and extinction) were converted to standard temperature and pressure (STP, 1 atm, 0°C) before data were uploaded. We used temperature and pressure measured by the PAS and CAPS PM_{SSA} to convert optical properties to STP. For absorption, the sample temperature measured by the PAS RH sensor (Vaisala RH probe) and the pressure measured by the temperature and pressure sensor of the CAPS PM_{SSA} were used. Whereas for extinction, temperature and pressure measured by the CAPS PM_{SSA} were used.~~

2.1.2 Cavity-Attenuated Phase Shift Spectrometer (CAPS PM_{SSA})

After pulling through the NO_X denuder, the $PM_{1.0}$ cyclone, and the Nafion drier in front of the PAS inlet, the sampled air entered through the Aerodyne CAPS PM_{SSA_450} and CAPS PM_{SSA_660} to measure the aerosol scattering and extinction coefficients at 450 nm and 660 nm, respectively. CAPS PM_{SSA} instruments measure extinction by utilizing the cavity attenuated phase shift spectroscopy and measure scattering with an integrating sphere (Onasch et al., 2015). Ammonium sulfate particles were used to calibrate the scattering channel of the CAPS PM_{SSA} during WE-CAN with an accuracy of +/- 3%.

2.1.3 Particle-into-Liquid Sampler (PILS) systems

BrC absorption and water-soluble organic carbon (WSOC) were measured by a Particle-into-Liquid Sampler (PILS) system (Sullivan et al., 2022). The PILS continuously collects ambient particles into purified water and provides a liquid sample with the aerosol particles dissolved in it for analysis (Orsini et al., 2003). The size-cut for the PILS was provided by a nonrotating microorifice uniform deposit impactor (MOUDI) with a 50% transmission efficiency of 1 μm (aerodynamic diameter) at 1 atmosphere ambient pressure (Marple et al., 1991). The total airflow for the PILS was approximately 15 LPM. Upstream of the PILS was an activated carbon parallel plate denuder (Eatough et al., 1993) to remove organic gases. In addition, a valve was manually closed periodically for 10 min diverting the airflow through a Teflon filter before entering the PILS allowing for background measurements. The liquid sample obtained from the PILS was pushed through a 0.2 μm PTFE liquid filter by a set of syringe pumps to ensure insoluble particles were removed. The flow was then directed through a liquid waveguide capillary cell (LWCC) and Total Organic Carbon (TOC) Analyzer for near real-time measurement of BrC absorption and WSOC, respectively. More details and a schematic illustration can be found in Zeng et al. (2021).

For the absorption measurement, a 2.5 m path-length LWCC (World Precision Instruments, Sarasota, FL) was used. A dual deuterium and tungsten halogen light source (DH-mini, Ocean Optics, Largo, FL) and absorption spectrometer (FLAME-T-UV-VIS, Ocean Optics, Largo, FL) were coupled to the LWCC via fiber optic cables. Absorption spectra were recorded using the Oceanview Spectroscopy Software over a range from 200 to 800 nm. The wavelength-dependent absorption was calculated following the method outlined in Hecobian et al. (2010). For this study, a 16 s integrated measurement of absorption with a limit of detection (LOD) of 0.1 Mm^{-1} was obtained (Sullivan et al., 2022).

For the WSOC measurement, a Sievers Model M9 Portable TOC Analyzer (Suez Waters Analytical Instruments, Boulder, CO) was used. This analyzer works by converting the organic carbon in the liquid sample to carbon dioxide through chemical oxidation involving ammonium persulfate and ultraviolet light. The carbon dioxide formed was then measured by conductivity. The increase in conductivity observed was proportional to the amount of organic carbon in the liquid sample. The analyzer was run in turbo mode providing a 4 s integrated measurement of WSOC with a LOD of 0.1 μg C/m^3 (Sullivan et al., 2022).

2.1.4 Single Particle Soot Photometer (SP2)

Refractory black carbon (rBC) number and mass concentrations were measured with a Single Particle Soot Photometer (SP2; Droplet Measurement Technologies) which uses a continuous, 1064 nm Nd:YAG laser to heat absorbing material, primarily rBC, to its vaporization temperature and measures the resulting incandescence (Schwarz et al., 2006). Similar to the CAPS PM_{SSA}, the sampled air was sent through the NO_X denuder, $PM_{1.0}$ cyclone, and Nafion drier in front of the PAS inlet before it went to the SP2. The SP2 was calibrated with PSL and size-selected fullerene soot. On the C-130, the SP2 sample line was diluted with HEPA-filtered, pressured ambient air that was passed through a mass flow controller to prevent signal saturation. During post-processing the data was corrected for dilution back to ambient concentrations ~~then to STP~~.

2.1.5 Ultra-High Sensitivity Aerosol Spectrometer (UHSAS)

Particle number concentration was measured by a rack-mounted Ultra-High Sensitivity Aerosol Spectrometer (UHSAS). The flow rate of the rack-mounted UHSAS can be manually lowered by the in-flight operator when the aircraft flew across smoke plumes, so that the UHSAS can stay within its optimum concentration measurement range (Sullivan et al., 2022). The UHSAS was calibrated with ammonium sulfate. The particle mass concentration was calculated by applying these size bins and multiplying by a particle density of 1.4 g cm^{-3} (Sullivan et al., 2022). The volume mean diameter of the particles for all the detected plumes range between 0.18 μm and 0.34 μm.

2.1.6 Proton-Transfer-Reaction Time-of-Flight Mass Spectrometer (PTR-ToF-MS)

The University of Montana proton-transfer-reaction time-of-flight mass spectrometer (PTR-ToF-MS 4000, Ionicon Analytik) was utilized to report the VOC mixing ratios during WE-CAN (Permar et al., 2021). Only the toluene and benzene mixing ratio derived from the PTF-ToF-MS were used in this work; their overall uncertainty is < 15%. More details of the operation, calibration, and validation on the PTR-ToF-MS during WE-CAN can be found in Permar et al. (2021).

2.1.7 High-Resolution Aerosol Mass Spectrometry (HR-AMS)

Organic aerosol (OA) was detected by the high-resolution aerosol mass spectrometry (HR-AMS; Aerodyne Inc.). The description of the AMS operation during WE-CAN can be found in Garofalo et al. (2019). The atomic oxygen-to-carbon ratios (O:C) and organic mass-to-organic carbon ratio (OM:OC) used in this work were determined via the improved ambient elemental analysis method for the AMS (Canagaratna et al., 2015). Average (integrated)

elemental ratios were obtained by averaging (integrating) elemental masses of carbon, hydrogen, and oxygen and recalculating elemental ratios.

2.1.8 Quantum Cascade Laser (QCL) and Picarro Cavity Ring-Down spectrometer (Picarro)

The carbon monoxide (CO) mixing ratio was measured by both an Aerodyne quantum cascade laser instrument (CS-108 miniQCL) and a Picarro cavity ring-down spectrometer (G2401-m WS-CRD) (Garofalo et al., 2019). Because the QCL has better precision than the Picarro instrument, CO measurements from the QCL were preferentially used. However, CO measurements from the Picarro CO data were used for RF10 and RF13, because the CO-QCL was not operated during those two flights. The carbon dioxide (CO_2) mixing ratio was also determined from the Picarro.

2.2 Plume Physical Age

The physical age of the plume was calculated by dividing the distance the plume was sampled from the fire source by the in-plume average wind speed. The average wind speed was measured on the NSF/NCAR C-130 aircraft during each plume pass. The distance was estimated by using the longitude and latitude of the geometric center of the plume measured on the NSF/NCAR C-130 and the fire location provided by the U.S. Forest Service. ~~These~~The same ~~plume ages were~~method was used by Garofalo et al. (2019), Peng et al. (2020), Lindaas et al. (2021), Permar et al. (2021), and Sullivan et al. ~~(2022).~~(2022) and are also utilized here for consistency.

2.3 Plume Integration Method

During the WE-CAN campaign, both the SP2 and PILS had ~~a~~ significant hysteresis compared to other instruments. In the SP2 this is because the sampled air was diluted with particle-free ambient air at various ratios to prevent signal saturation. In the PILS this is because of the retention effect of liquid on the wetted component or within dead volumes (Zeng et al., 2021). Therefore, it was most accurate to integrate properties across airborne transects of wildfire plumes to avoid the impact of instrument hysteresis and measurement noise that can dramatically impact instantaneous ratios. Pseudo-Lagrangian sampling was used during the flights for the WE-CAN campaign, the C-130 aircraft repeatedly crossed the smoke plume from a particular fire by traveling perpendicular to the prevailing winds, crossing the plume, turning, then crossing the plume again further downwind. In this work, we manually identified plume edges based on the inflection point when CO concentrations stopped rapidly changing as we entered and exited the smoke plume. The outside of plume measurement periods had CO mixing ratios from 100 - 300 ppbv. The lowest 10% of each variable from outside plume segments were set to be the background of that variable. If the time between two consecutive outside plume segments was larger than 20 s and the highest CO mixing ratio was 100 ppbv higher than the outside plume CO criteria, this segment was chosen as a plume. The start and end point of each plume was slightly adjusted manually based on the CO mixing ratio to make sure the entire plume was covered. A different start and end point for the SP2 and PILS was adjusted manually based on the rBC mass concentrations and WSOC, respectively.

2.4 Absorption Enhancement and Mass Absorption Cross-section

Absorption enhancement (E_{abs}) is the ratio of the absorption of ~~the whole particle~~all particles (including BC core and coating materials) to the absorption of ~~the~~ BC ~~core~~alone (Lack and Cappa, 2010). E_{abs} at a specific wavelength (E_{abs_λ}) was calculated in this study by Eq. ~~1~~2:

$$E_{abs\_\lambda} = \frac{\beta_{Total\_\lambda}}{M_{BC} * MAC_{BC\_core\_\lambda}} \frac{Abs_{Total\_\lambda}}{M_{BC} * MAC_{BC\_core\_\lambda}} \quad (Eq.\ 1\text{~~}2) \quad (Eq.\ 12)$$

where ~~β_{Total_λ}~~Abs_{Total_λ} is the total absorption coefficient at a wavelength of λ nm measured by the PAS, M_{BC} is the mass concentration of BC measured by the SP2, and $MAC_{BC\_core\_\lambda}$ is the MAC of BC ~~core~~alone (without any other coating material) at λ nm, which is set to be 6.3 $m^2\ g^{-1}$ at 660 nm (Bond and Bergstrom, 2006; Subramanian et al., 2010).

MAC_{BC} at λ nm was calculated following Eq. ~~2~~3:

$$MAC_{BC\_\lambda} = \frac{\beta_{Total\_\lambda}}{M_{BC}} \frac{Abs_{Total\_\lambda}}{M_{BC}} \quad (Eq.\ 2\text{~~}3) \quad (Eq.\ 23)$$

MAC_{BC_λ} is utilized more often in this study than E_{abs} because there is not a widely accepted MAC for BC emitted from wildfire. MAC of BrC and lensing is calculated at 405 and 660 nm (Eq. ~~3~~4):

$$MAC_{BrC+lensing\_\lambda} = \frac{\beta_{Total\_\lambda} - M_{BC} * MAC_{BC\_core\_\lambda}}{M_{OA}} \frac{Abs_{Total\_\lambda} - M_{BC} * MAC_{BC\_core\_\lambda}}{M_{OA}} \quad (Eq.\ 3\text{~~}4) \quad (Eq.\ 34)$$

where M_{OA} is the organic mass measured by the AMS. Again, the ~~MAC of the BC~~ $MAC_{BC\_core\_\lambda}$ is set to be 6.3 and 10.2 $m^2\ g^{-1}$, respectively, at 660 nm and 405 nm yielding an absorption Ångström exponent (AAE, the negative slope of a logarithmic absorption coefficient against wavelength) of 0.99 for the BC core (Bond and Bergstrom, 2006; Subramanian et al., 2010; Liu, et al., 2015). It should be noted that both BrC and lensing contribute to the $MAC_{BrC+lensing}$, and cannot be separated using this approach. MAC of water-soluble BrC at ~~660~~λ nm ($MAC_{ws\_BrC\_660}$~~)~~$_\lambda$) is calculated using Eq. ~~4~~5:

$$MAC_{ws\_BrC\_660} = \frac{\beta_{ws\_BrC660}}{WSOC} MAC_{ws\_BrC\lambda} = \frac{Abs_{ws\_BrC\_\lambda}}{WSOC * (\text{WSOM: WSOC})} \quad (Eq.\ 4\text{~~}5) \quad (Eq.\ 45)$$

where ~~β_{ws_BrC660}~~$Abs_{ws\_BrC\_660}$ is water-soluble light absorption and WSOC is water-soluble organic carbon mass, which are both measured by the PILS system. WSOM:WSOC ratio is set to be 1.6 (Sullivan et al., 2022).

~~To investigate which contributes more to absorption enhancement at 660 nm, the absorption from BrC or the lensing effect, the fractional absorption from BrC at 660 nm is calculated by Eq. 5~~

$$Fractional\ Abs_{BrC} = \frac{\beta_{BrC\_660}}{\beta_{Total\_660} - M_{BC} * MAC_{BC\_core\_660}} \quad (Eq.\ 5)$$

where β_{BrC_660} is the total BrC absorption coefficient at 660 nm. This is calculated from the water-soluble light absorption provided by the PILS, where we convert absorption from water-soluble BrC to total BrC by WSOM:WSOC and OM:WSOM ratio, and correct absorption from liquid phase to particle phase via Mie theory (more details in 3.1.4, Eq. 9-10). 2.5 Fractional non-BC Absorption from BrC

This approach assumes that water insoluble BrC has the same refractive index as water soluble BrC. This assumption would provide a lower estimation on the BrC contribution to the total absorption because Sullivan et al. (2022) found that 45% of the BrC absorption at 405 nm in WE-CAN came from water-soluble species, and Zeng et al. (2022) found that insoluble BrC absorbs more at higher wavelengths than soluble BrC, and methanol-insoluble BrC chromophores caused 87% of the light absorption at 664 nm. β_{Total_660} is the total absorption coefficient at 660 nm which is measured by the PAS, M_{BC} is the mass concentration of BC which is measured by the SP2, and $MAC_{BC\_core\_660}$ is the MAC of the BC core at 660 nm which is set to be 6.3 $m^2 \cdot g^{-1}$ (Bond and Bergstrom, 2006; Subramanian et al., 2010).

2.5 Modified Combustion Efficiency (MCE)

The variation of burn condition (e.g., flaming vs. smoldering) and fuel type can cause a significant difference in BC emissions and changes in aerosol properties (Akagi et al., 2011; Andreae, 2019). Burn conditions can be estimated with the modified combustion efficiency (MCE), defined as Eq. 6:

$$MCE = \frac{\Delta CO_2}{\Delta CO + \Delta CO_2} \quad (Eq. 6)$$

where ΔCO_2 and ΔCO are the background subtracted CO_2 and CO mixing ratio. The background of CO_2 and CO mixing ratio is obtained via the same process described in Section 2.3.

2.6 Absorption, Scattering and Single Scattering Albedo (SSA)

Plume-integrated absorption and scattering were normalized (x/CO) by taking the ratio of background-subtracted absorption or scattering (Δx) to the background subtracted CO mixing ratio (ΔCO) (Eq. 7), so that the changing of the normalized properties is not impacted by dilution of the plume with background air.

$$x/CO = \frac{\Delta x}{\Delta CO} \quad (Eq. 7)$$

Although the CAPS PM_{SSA} provides scattering directly, the scattering is only accurate if extinction is below 1000 Mm^{-1} (Onasch et al., 2015). We calculated scattering by subtracting absorption measured by the PAS from extinction measured by the CAPS PM_{SSA} to avoid high uncertainty caused by extremely dark plumes. Similarly, SSA at a specific wavelength (λ) was also calculated by using both the PAS absorption (β_{Total_λ}) and CAPS PM_{SSA} extinction (Ext_λ) (Eq. 8).

$$SSA_\lambda = \frac{Ext_\lambda - \beta_{Total\_\lambda}}{Ext_\lambda} \quad (Eq. 8)$$

3 Results and Discussion

3.1 Absorption of BC and BrC at Red Wavelengths

3.1.1 Mass Absorption Cross-Section of Black Carbon at 660 nm

Plume-integrated MCE, MAC_{BC} at 660 nm (MAC_{BC660}) and BC:OA ratio from the 13 WE-CAN research flights with clear plume transects of biomass burning plumes are shown in Fig. 2. Even fire plumes from individually named fires are usually a mix of many different burning conditions, and it is hard to identify the exact source in most wildfire smoke measurements, especially for well-mixed plumes. Therefore flight-to-flight data is analyzed in this study because each flight covered a region, and an overall behavior of absorbing aerosol from wildfire can be provided. MAC_{BC660} varies between different flights with RF03 having the highest average MAC_{BC660} of 12.9 $m^2 g^{-1}$, (median MCE of 0.94, median BC:OA of 0.015) and RF10 having the lowest average MAC_{BC660} of 8.6 $m^2 g^{-1}$, (median MCE of 0.88, , median BC:OA of 0.011). The average of all plume-integrated MAC_{BC660} is 10.9 $m^2 g^{-1}$, with a standard deviation of 2.1 $m^2 g^{-1}$. This result is similar to some other recent airborne measurements. Subramanian et al. (2010) reported a MAC_{BC660} of 10.9 ± 2.1 $m^2 g^{-1}$ using a SP2 and PSAP operated during the MILAGRO campaign, which included airborne measurements for biomass fires over Mexico. Similarly, Zhang et al. (2017) estimated a MAC_{BC660} of 10 $m^2 g^{-1}$ utilizing both SP2 and PSAP deployed on the NASA DC-8 research aircraft for the DC3 campaign, which measured the upper tropospheric BC over the central U.S. Taylor et al. (2020) calculated a MAC_{BC655} of 12 ± 2 $m^2 g^{-1}$ over the southeast Atlantic Ocean, using airborne measurements from a SP2 and PAS in the CLARIFY 2017 campaign.

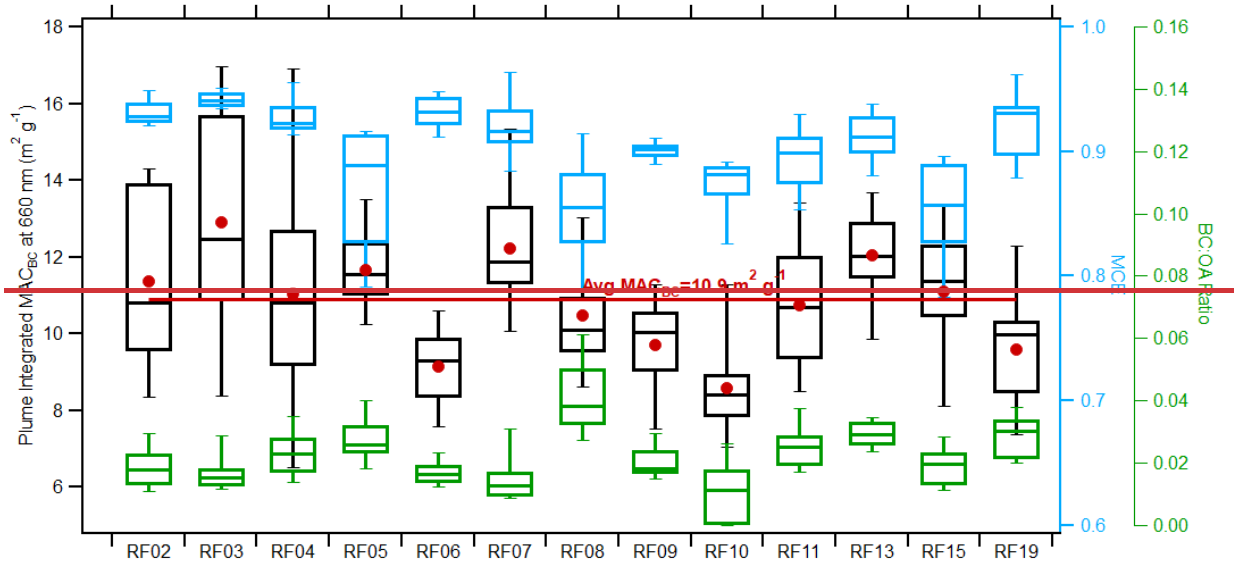

Figure 2: Box plots of plume integrated MCE (blue box), MAC_{BC660} (black box) and BC:OA (green box) for each flight. On each box the central line represents the median, the top and bottom edge represents 75% and 25%, the top and bottom whiskers represent 90% and 10%, and the red dot shows the average. The red line indicates the average value for all plume integrated MAC_{BC660}.

These results are encouragingly similar given the breadth of measurement techniques (PSAP is filter-based whereas PAS is a direct measurement), geographic regions (Continental U.S. for DC3, Mexico for MILAGRO, African outflow for CLARIFY) and altitude in the atmosphere (all were airborne campaigns covering a range of altitudes). If

we apply 6.3 $m^2 g^{-1}$ as the MAC of a BC core at 660 nm (Bond and Bergstrom, 2006; Subramanian et al., 2010), then the average absorption enhancement for the entire campaign is 1.7. This means the absorption of coated BC is 1.7 times higher than bare BC at 660 nm, which is close to the factor of ~2 reported by laboratory experiments (Schnaiter et al., 2005; Peng et al., 2016), larger than some field measurements (Cappa et al., 2012&2019; Healy et al., 2015), but close to 1.85 ± 0.45 measured by Taylor et al. (2020) in African biomass burning plumes. The similarity to the Taylor et al. (2020) result suggests global similarities in the MAC_{BC660} from aerosol emitted from wildfires.

The variation of MCE in different flights is caused by the different fuel sources and burning characteristics of the measured fires. Fires with high MCE tend to have more flaming combustion while those with lower MCE tend to have more smoldering combustion. Because of this, fires with different MCE may produce different coating material and thus changing MAC_{BC660}. MCE can vary in the same flight (Fig. 2), for example RF05 (mixture of multiple fire sources) and RF15 (single fire sources), because multiple fires were measured in some flights. Several other factors, such as physical age and chemical age (discussed later) also may impact MAC_{BC660}, but we first investigate if there was a clear relationship between MCE and MAC_{BC660}.

The comparison between plume integrated MAC_{BC660} and MCE is shown in Fig. S1. No clear relationship between MAC_{BC660} and MCE can be seen from individual flights or amongst all the flights combined (R^2=0.01). This result indicates that the combustion conditions (flaming or smoldering) does not have an easily described relationship to MAC_{BC660}. This poor relation is similar to the relationship observed by Pokhrel et al. (2016). This lack of relationship is likely due to the difficulty for MCE to predict aerosol properties such as BC:OA (Grieshop et al., 2009), upon which effective organic aerosol absorptivity highly depends (Saleh et al., 2014).

3.1.2 Relationship of Bulk Optical Properties at 660 nm to Physical Age

Figure 3 shows the evolution of MAC_{BC660}, SSA, scattering and absorption at 660 nm versus the time since emission, which will be referred to from now on as physical age. While some flights only intercepted fresh plumes (for example, RF03 and RF15, with a physical age less than 200 min), others intercepted relatively old plumes (for example, RF02 and RF11, with a physical age of 600 min and 800 min, respectively). To eliminate the influence of dilution of particles with time, scattering and absorption are normalized by taking the ratio of the enhancement of scattering or absorption above the background to the enhancement of CO concentration above the background. CO is a conserved tracer that does not react on timescales relevant to these observations. No clear trend between MAC_{BC660} and physical age is apparent from individual flights (Fig. 3a), linear fitting of all flights combined (black solid line) gives a slope close to zero demonstrating that the absorption enhancement changes little with physical age, which is consistent with the results from Subramanian et al. (2010).

However, SSA at 660 nm (SSA_{660}) shows a slightly increasing trend with physical age (Fig. 3b) increasing from 0.94 to 0.97 in 10 hours, though the correlation is not very strong with a R^2 of 0.14. The increase of SSA_{660} is partly caused by the increase of scattering at 660 nm (Fig. 3c). The particle size increases with age (Fig. S2) due to coagulation of small particles and condensation of vapors. The volume mean diameter of the particles increased from on average 0.18 μm to 0.34 μm across all the plumes detected. Even for each individual flight, the increasing trend in particle mean diameter is clear. Another contributor to increasing SSA is the decrease in absorption at 660 nm (Fig.

3d) with age for most fires. Overall, the trends in SSA, absorption, and scattering with physical age are quite weak with poor correlation coefficients.

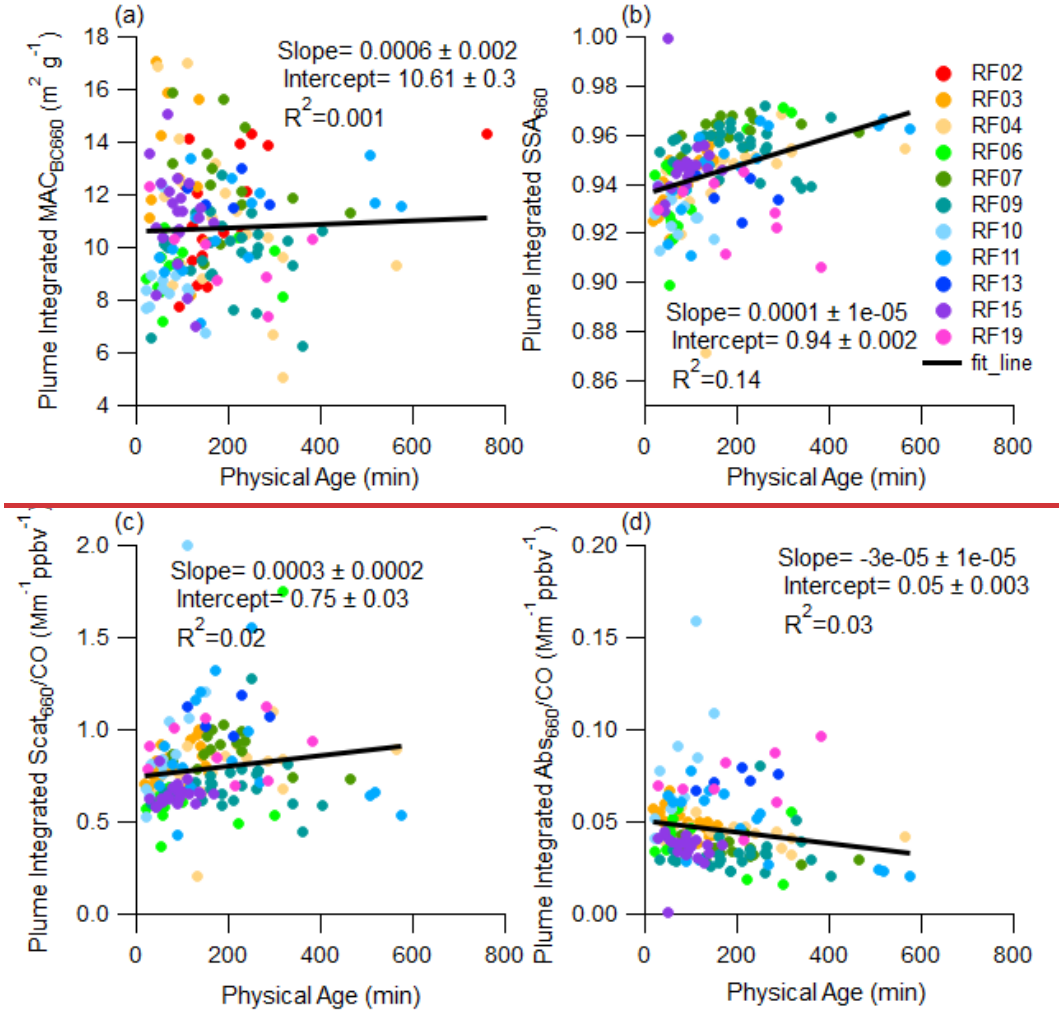

Figure 3: Time evolution of plume integrated (a) MAC_{BC660}, (b) SSA_{660}, (c) scattering, and (d) absorption at 660 nm.

3.1.3 Response of Optical Properties at 660 nm to Markers of Chemical Oxidation

MAC_{BC660} was next compared to chemical markers of oxidation, since physical age did not provide strong correlations and often does not do a good job of representing oxidation and photochemical reactions that occur in plumes. Organic coatings of BC cores may be removed via these reactions, or new species may condense on the BC core during chemical reactions, both of which would further change the optical properties of BC. Figure 4 shows the evolution of plume integrated MAC_{BC660} versus chemical clocks based on (a) the ratio of gas-phase toluene:benzene and (b) the particle-phase oxygen-to-carbon (O:C) ratio. The toluene:benzene ratio decreases with photochemical processing time since toluene is more reactive than benzene (Gouw et al., 2005), while The O:C ratio characterizes the oxidation state of OA and typically increases with photochemical age (Aiken et al., 2008).

As shown in Fig. 4 the toluene:benzene ratio ranges from 0.33 to 0.88 across all flights while the O:C ratio is between 0.35 and 0.72. It is difficult to discern any pattern of MAC_{BC660} changing with either marker in an individual flight. However, the trends are slightly clearer after combining plumes from all the flights. From the linear fit line (black solid line) to data from all flights, the negative slope of -5.7 between MAC_{BC660} and toluene:benzene ratio (Fig. 4a) infers that MAC_{BC660} is larger when toluene:benzene is lower, which is typically thought to indicate more extensive oxidation has occurred. The positive slope of 2.2 between MAC_{BC660} and O:C ratio (Fig. 4b), supports the idea of larger MAC_{BC660} with more oxidation. However, correlations are poor (R^2 < 0.2) and because these trends are not visible within a single plume, the explanation for the trends must be either that different fires emit different O:C and toluene:benzene ratios, or that the chemistry that created the observed ratios occurred before the first transect of a plume. Figure S3 supports this explanation in that while there is chemical aging within flights, the O:C and toluene:benzene ratios are more variable from flight to flight. For example, RF06 got more chemical aged with time, but the chemical markers for RF13 were flat with time. For either mechanism, the data shows that plumes that appear "older" either by photochemical aging or because of more aged appearing emissions have a slightly higher MAC_{BC660}, though the main point is that the MAC_{BC660} does not change dramatically with either physical or chemical age for the observations during WE-CAN.

Figure 4c and 4d show that the plume-integrated mass concentration of BC (M_{BC}, from the SP2) normalized by CO (the ratio of background subtracted M_{BC} to background subtracted CO) decreases with the toluene:benzene and O:C ratios. One would expect a constant value of M_{BC}/CO for single plumes from an individual fire because both are primary and inert. Indeed, there is no obvious decreasing of M_{BC} (R^2 <0.5) within an individual flights except for RF13. The decreasing of M_{BC} with markers of chemical age amongst all the flights appears to be due to the different properties of the different fires near the source. Different fires tend to have different O:C ratio and toluene:benzene ratios, as shown in Fig. S4. Therefore, the decreasing trend of M_{BC} with markers of chemical age is more likely caused by fire-to-fire properties or rapid aging at the source rather than aging of the plume after the initial transect.

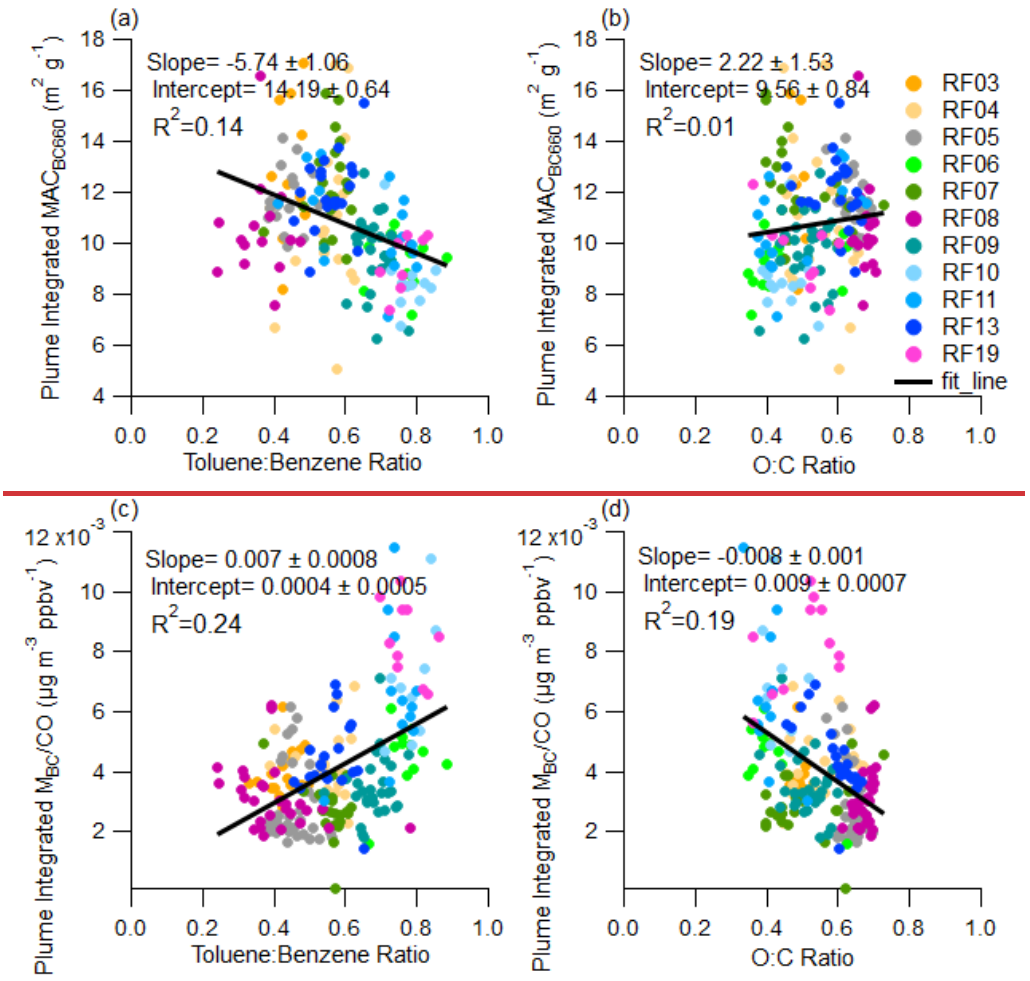

~~Figure 4: Plume integrated MAC_{BC660} variations with (a) toluene:benzene ratio and (b)O:C ratio; plume integrated M_{BC} variations with (c) toluene:benzene ratio and (d)O:C ratio.~~

~~SSA, scattering, and absorption at 660 nm are compared with the toluene:benzene ratio and O:C ratio in Fig. 5. There is a slight trend of increasing SSA_{660} with these ratios that would correspond to more oxidized aerosol, but the correlation is poor (R^2=0.04). The increase of SSA_{660} with markers of chemical age is consistent with the work from Kleinman et al. (2020) on Western U.S. wildfire emissions, although $Log_{10}(NO_x/NO_y)$ was used as the indicator for photochemical age in their study.~~

~~Both scattering and absorption at 660 nm decrease with ratios corresponding to more chemical aging, which suggests that the amount of absorbing material has changed. The comparison between normalized OA and these markers of chemical age demonstrates that this is indeed the case. As can be seen in Fig. 5 (g-h), OA decreases with increasing O:C ratio with an R^2 of 0.7. A similar relationship can be found between normalized WSOC chemical age (Fig. 6) in that WSOC decreases with increasing O:C ratio with a R^2 of 0.3. However, it is key to note that this correlation is not derived from individual flights and in fact is not robust in each flight and is rather due to fire-to-fire variation. Figure S5 shows the correlation between normalized OA and chemical age within each fire source, which shows that different fires emit different OA, and OA does not always decrease with chemical age within a single fire~~

~~(Kiwah fire and Rabbitfoot fire). Therefore, we believe that different OA is caused by fire properties or fast chemistry near the source, but that these markers (O:C, toluene:benzene) provide a significant correlation with the amount of organic aerosol observed in various plumes.~~

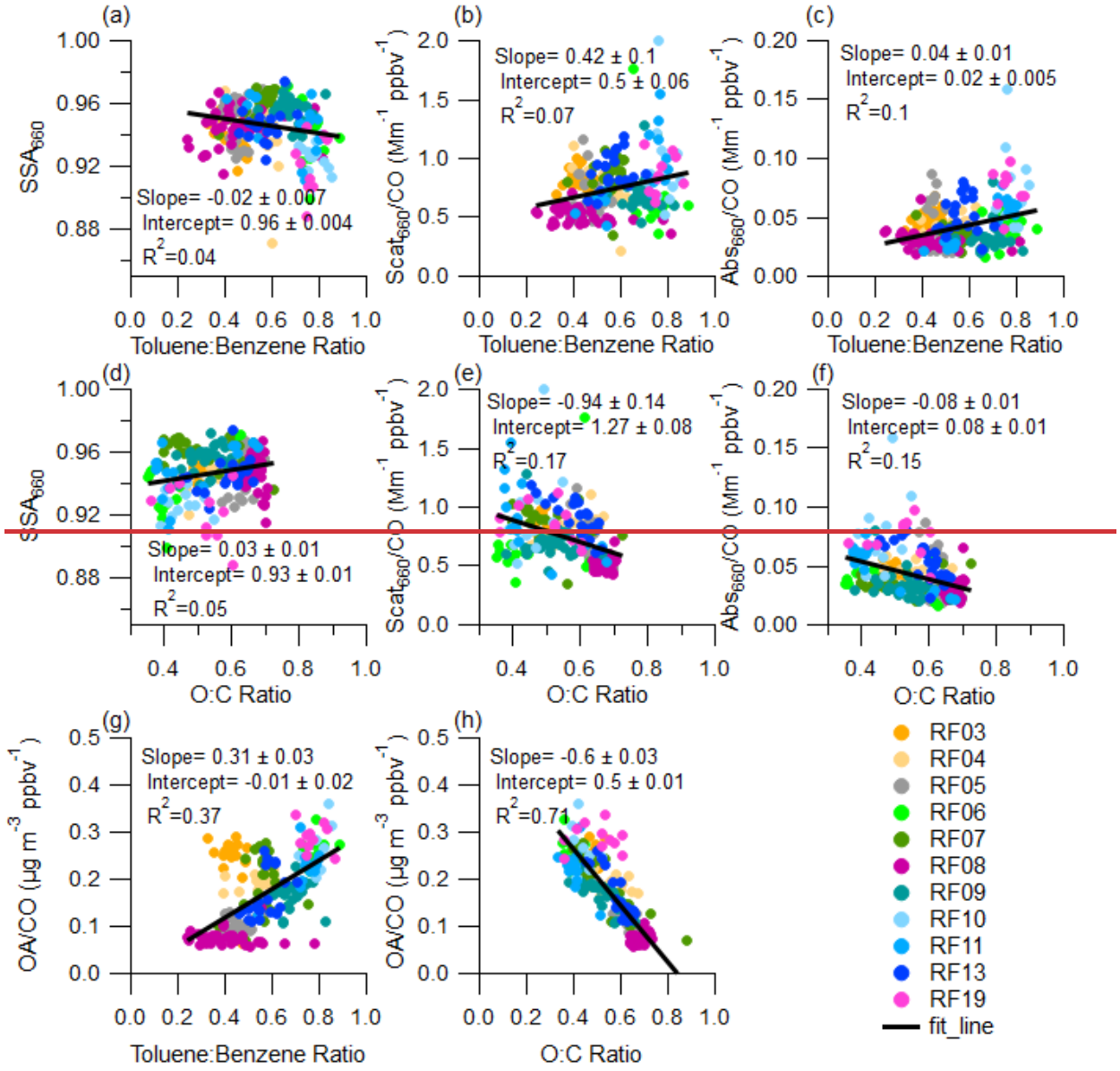

~~Figure 5: Plume integrated optical properties at 660 nm and normalized OA variation with chemical age. Top panels show (a) SSA, (b) Scattering, and (c) absorption variation with toluene:benzene ratio. Middle panels show (d) SSA, (e) Scattering, and (f) absorption variation with O:C ratio. Bottom panels show plume integrated normalized OA variation with (g) toluene:benzene ratio and (h) O:C ratio.~~

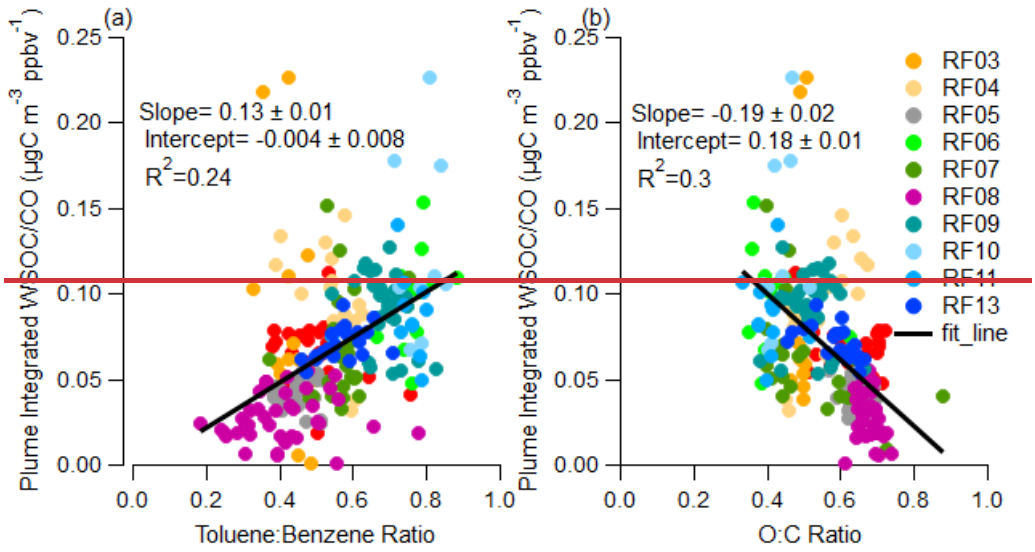

~~**Figure 6: Plume integrated normalized WSOC variation with (a) toluene:benzene ratio and (b) O:C ratio.**~~

~~The behavior of plume integrated normalized OA with altitude and temperature is shown in Fig. 7 a-b. The trend is not significant, but the main reason is that for most flights we transected the plume, and caused the straight lines within the same colored marker. However, it is still clear that the smallest OA was captured in the plumes (RF08) that have highest temperature (~305 K), and larger OA tends to be observed in the colder plumes (RF19). More studies are needed to determine whether OA is evaporated in high temperature plume, but it's beyond the scope of this work.~~

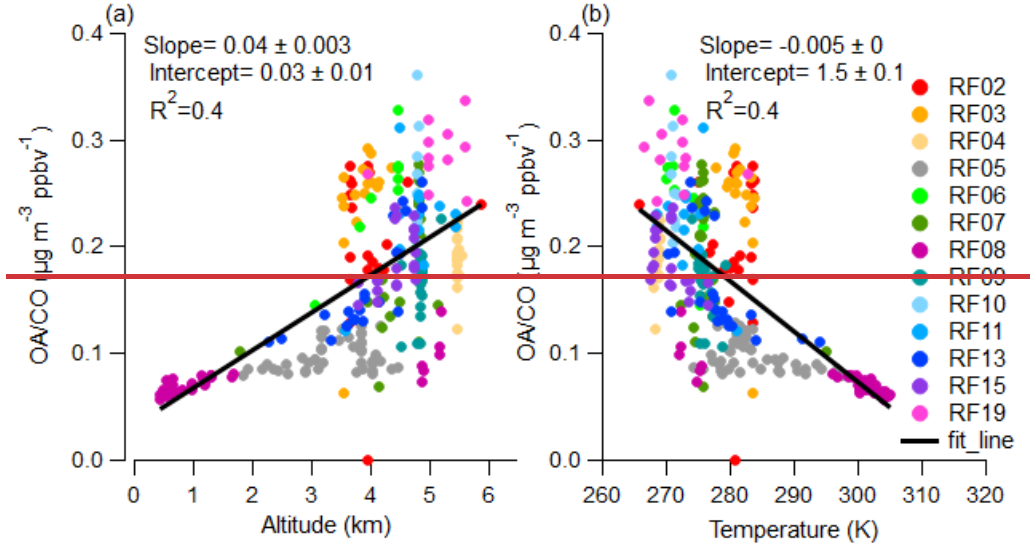

~~**Figure 7: Plume integrated normalized OA variation with (a) altitude and (b) temperature.**~~

~~RF05 and RF08 were chosen as case studies, to observe the optical properties of highly aged aerosol from multiple fire sources to see if the optical properties of this aerosol were similar to those observed in the plume sampling of individual fires at large chemical or physical age. RF08 was a flight through the Central Valley of California where aged smoke from multiple fires that had settled into the valley was measured while RF05 was a flight in which smoke~~

from several California fires was observed in California, Oregon and Idaho roughly 300–600 miles from the fires (flightpaths are shown in Fig. 1). MAC_{BC660}, CO mixing ratio, MCE, toluene:benzene ratio, O:C ratio and SSA_{660} are displayed in Fig. 8a and 8b. The mixing ratio of CO is relatively low in these aged dilute smoke plumes vs. the plumes near the sources analyzed earlier. CO mixing ratio is used as an indicator of smoke when it exceeds 150 ppb. 1-minute averages of MAC_{BC660} are calculated to reduce noise. Therefore, the 1-minute averages for MCE, toluene:benzene ratio and O:C ratio were also calculated, and all the negative values were removed. As shown in Fig. 8, the smallest toluene:benzene ratio is ~0.35 in RF05, and is ~0.16 in RF08, while the largest O:C ratio is ~0.7 in both RF05 and RF08, which indicates these two cases indeed captured plumes that appear chemically aged compared with the smallest toluene:benzene ratio (0.33) and the largest O:C ratio (0.88) in near-fire measurements shown in Fig. 4.

In RF05 (Fig. 8a), the weighted average O:C ratio over the entire flight was 0.64, the average MCE was 0.82 with a standard deviation of 0.1, the toluene:benzene ratio averaged 0.45 with a standard deviation of 0.05, and the SSA_{660} averaged 0.95 with a standard deviation of 0.01. MCE has a few points because all the negative values were removed, where either CO or CO2 is smaller than the background (CO < 150 ppb). MAC_{BC660} varied from 8.9 $m^2 g^{-1}$ to 15.7 $m^2 g^{-1}$ with an average of 11.7 $m^2 g^{-1}$ and a standard deviation of 1.38 $m^2 g^{-1}$. The reasonably large variation of MCE may be caused by variability in the burn conditions of different fire sources, but the overall conclusion is that these emissions, which were measured 300 to 600 miles away, have a very similar MAC_{BC660} to that of the near-source flights.

The RF08 (Fig. 8b) results are similar to RF05, even though these emissions were smoke of mixed aged from multiple fire sources in the Central Valley. The weighted average O:C ratio was 0.67 over the entire measurement, average MCE was 0.84 with a standard deviation of 0.05, average toluene:benzene ratio was 0.41 with a standard deviation of 0.15, and average SSA_{660} was 0.94 with a standard deviation of 0.01. MAC_{BC660} averaged 10.9 $m^2 g^{-1}$ with a standard deviation is 2.24 $m^2 g^{-1}$. There are several extreme values that exist in the dataset, probably because of time alignment issues caused by variation in the dilution rate of the SP2 which cannot be totally eliminated from the 1-minute average. In addition, the smoke from RF08 (Fig. 8b) is split into four regions based on observed CO mixing ratios, and integrated MAC_{BC660} is calculated for each region (purple star marker). Region edges are represented by blue dashed lines. Region integrated MAC_{BC660} is relatively stable with an average value of 10.2 $m^2 g^{-1}$ and a standard deviation of 0.6 $m^2 g^{-1}$.

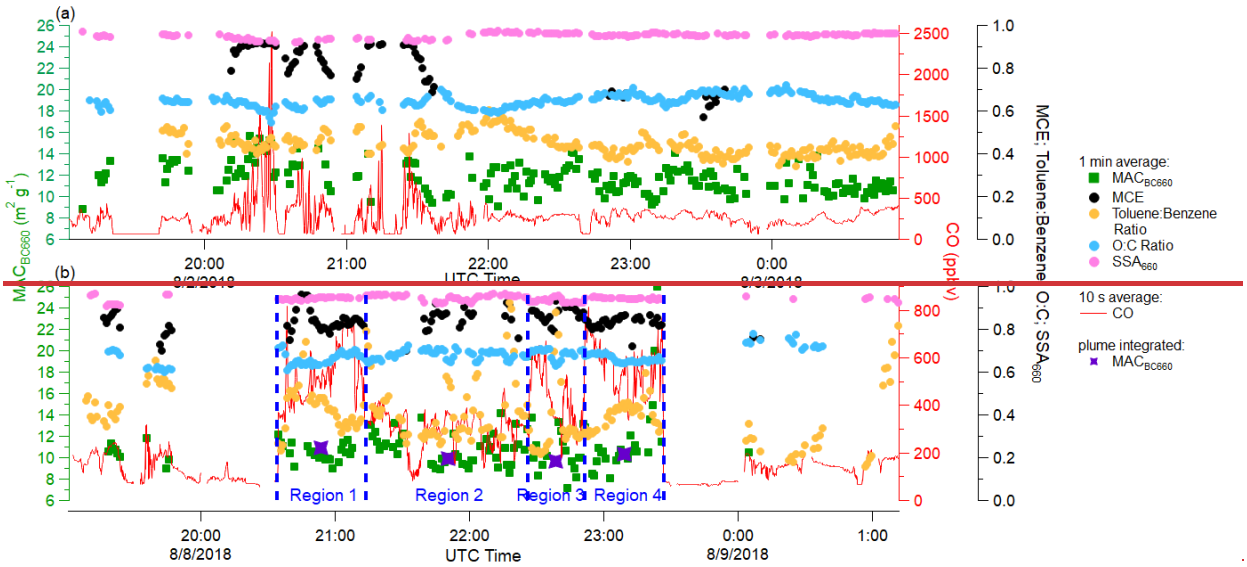

~~Figure 8: Time series of plume properties during (a) RF05, and (b) RF08(Central Valley of California). Different square and round markers indicate 1-min averages of different variables as shown in the legend, and the red solid line represents 10-s averages of the mixing ratio of CO.~~ ~~Purple stars in RF08 indicate region integrated MAC$_{BC660}$ (individual regions are separated based on the concentration of CO, and indicated by blue dashed lines).~~

~~The behavior of plume-integrated MAC$_{BC660}$ with altitude and temperature is shown in Fig. 9 a-b. MAC$_{BC660}$ shows little correlation with altitude or temperature, even though there is a large range of both (altitude 500 m to 6 km, temperature 270 K to 305 K). To assess the impact from dilution, the relation between MAC$_{BC660}$ and ΔCO is shown in Fig. 9c. The MAC$_{BC660}$ may decrease slightly with dilution (lower ΔCO), but the correlation is very poor. Neither altitude, temperature, or dilution appear to have a dramatic impact on the MAC$_{BC660}$.~~

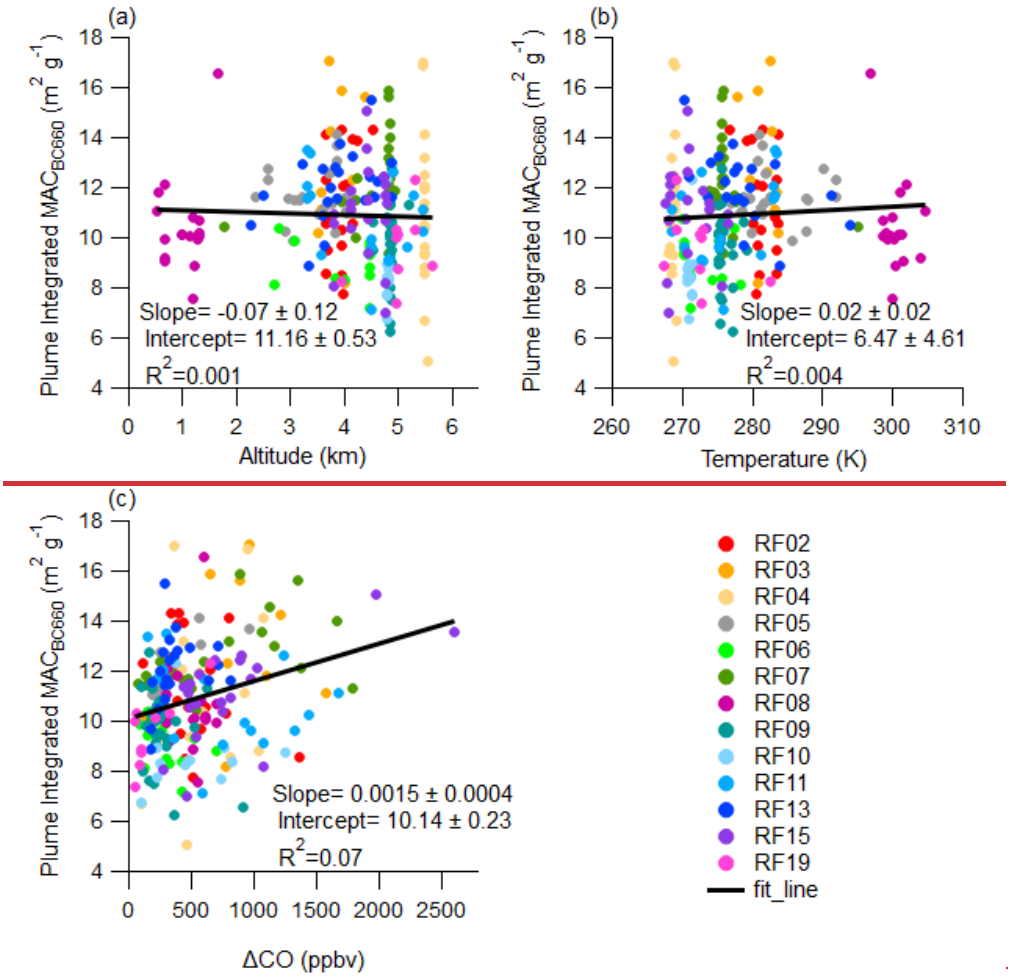

~~**Figure 9: Plume integrated MAC_{BC660} variations with (a) Altitude, (b) Temperature, and (c) ΔCO.**~~

~~3.1.4 Contribution of Brown Carbon Versus Lensing at 660 nm~~

Many previous studies of BrC assume that BrC does not absorb significant amounts of light at long wavelengths (532~705 nm) (Wonaschütz et al., 2009; Lack et al., 2012a; Taylor et al., 2020; Zeng et al., 2021, Zhang et al., 2022). In this study, a PILS system was used to quantify the absorption of light for water-soluble BrC at 660 nm. This absorption is not likely caused by traditional BC, which is insoluble and will be removed by the 0.2 μm filter in the PILS (Peltier et al., 2007; Zeng et al., 2021).

~~One aim was~~ To investigate ~~if~~ which contributes more to absorption enhancement at 660 nm ~~was primarily due to,~~ the ~~lensing effect or due to~~ absorption from BrC~~. The fraction of~~ or the lensing effect, the fractional non-BC absorption from BrC at 660 nm ~~was~~is calculated by Eq. 6

$$Fractional\ Abs_{BrC} = \frac{Abs_{BrC\_660}}{Abs_{Total\_660} - M_{BC} * MAC_{BC\_core\_660}} \quad (Eq.\ 6)$$

where Abs_{Total_660} is the total absorption coefficient at 660 nm which is measured by the PAS, M_{BC} is the mass concentration of BC which is measured by the SP2, and $MAC_{BC\_core\_660}$ is the MAC of the BC core at 660 nm which

is set to be 6.3 m^2 g^{-1} (Bond and Bergstrom, 2006; Subramanian et al., 2010). ~~5.~~Abs_{BrC_660} is the total BrC absorption coefficient at 660 nm, which is calculated from the water-soluble light absorption provided by the PILS, where we convert absorption from water-soluble BrC to total BrC. More specifically, to convert the measured light absorption by water-soluble organics into total BrC absorption in the ambient, it had to be multiplied by two factors. The first factor converts absorption from water-soluble BrC into absorption from total BrC. This factor is obtained by taking the ratio between total particulate organic mass and water-soluble particulate organic mass (OM:~~WSOC~~WSOM). Water-soluble organic mass is calculated from the PILS WSOC data using a WSOM:WSOC (water-soluble organic mass : water-soluble organic carbon) ratio of 1.6 (Duarte et al., 2015 & 2019). Ambient organic mass is measured by the AMS or calculated from the particle size distributions measured by the UHSAS assuming the particle mass all comes from organic material with a particle density of 1.4 g cm^{-3}. Both methods are used and compared in this paper. The second factor accounts for the fact that particles absorb more light than the same substance in the bulk liquid phase. Here we use Mie theory (Bohren and Huffman, 1983) to convert absorption from BrC in aqueous solution to the absorption from BrC particles in the ambient (Liu et al., 2013; Zeng et al., 2020). The complex refractive index (m = n+ *i*k) was put into a Mie code (implemented into Igor by Ernie R. Lewis base on Bohren and Huffman, 1983) to obtain the absorption efficiency (Q), and further used to calculate the absorption coefficient by Eq. ~~9~~7 (Liu et al., 2013). The real part of the refractive index (n) is set to be 1.55, and the imaginary part is calculated by using Eq. ~~10~~8 (Liu et al., 2013~~),~~).

$$\beta Abs\left(\lambda, D_p\right) = \frac{3}{2} \cdot \frac{Q \cdot WSOC}{D_p \cdot \rho} \quad (Eq.\ 9)$$

$$k = \frac{\rho\lambda \cdot H_2O\_\beta(\lambda)}{4\pi \cdot WSOC} k = \frac{\rho\lambda \cdot H_2O\_Abs(\lambda)}{4\pi \cdot WSOC} \quad (Eq.\ 10)$$

where λ is the wavelength, D_p is the diameter of the particle, $\beta Abs\left(\lambda, D_p\right)$ is absorption coefficient, Q is absorption efficiency, particle density (ρ) is set to be 1.4 g cm^{-3}, $WSOC$ is the mass concentration of WSOC (μgC m^{-3}) measured by the PILS, and $H_2O\_\beta Abs(\lambda)$ is the water-soluble light absorption coefficient measured by PILS. The plume averaged particle size distribution was used in the calculation, then the absorption coefficient was calculated for each size bin of UHSAS to obtain the most accurate Mie factor for each plume.

The average OM:~~WSOC~~WSOM factor based on the UHSAS (UHSAS factor) for all the plumes is 2.36 with a standard deviation is 1.17. The averaged OM:~~WSOC~~WSOM based on the AMS (AMS factor) is 1.63 with a standard deviation of 0.74. The average Mie factor at 660 nm is 1.47 (standard deviation of 0.13), which is close to the factor of 1.36 found by Zeng et al. (2022) based on FIREX data. The Mie factor at 405 nm based on the WE-CAN data is also calculated, with an average of 1.83, which is similar to the factor that Zeng et al. (2022) determined at 405 nm (1.7) based on FIREX and Liu et al. (2013) determined at 450 nm (1.9) based on measurements in Atlanta.

Sensitivity tests were done on these factors by choosing reasonable ranges of particle density (1.1 g cm^{-3}, 1.4 g cm^{-3} and 1.7 g cm^{-3}) and WSOM:WSOC ratio (1.5, 1.6 and 1.8) (Duarte et al., 2015 & 2019; Finessi, et al., 2012; Sun et al., 2011) (Table ~~1~~S1). Particle density only affects the Mie factor and UHSAS factor, while WSOM:WSOC

ratio affects the AMS factor and UHSAS factor. As shown in Table ~~1~~S1, the impact of particle density on the Mie factor (both at 660 nm and 405 nm) is negligible, WSOM:WSOC is the only component that affects the AMS factor (ranging from 1.48 to 1.73), while the UHSAS factor is much more sensitive (ranging from 1.65 to 3.06) to both particle density and WSOM:WSOC. Overall, Table ~~1~~S1 demonstrates that none of the factors other than the UHSAS factor are sensitive to the exact parameters chosen for the calculation, giving confidence that the results presented are robust.

This approach assumes that water insoluble BrC has the same refractive index as water soluble BrC. This assumption would provide a lower estimation on the BrC contribution to the total absorption because Sullivan et al. (2022) found that 45% of the BrC absorption at 405 nm in WE-CAN came from water-soluble species, and Zeng et al. (2022) found that insoluble BrC absorbs more at higher wavelengths than soluble BrC, and methanol-insoluble BrC chromophores caused 87% of the light absorption at 664 nm.

2.6 Absorption of BrC and Water-soluble BrC

The bulk absorption coefficient of water-soluble BrC at a specific wavelength ($Abs_{ws\_BrC\lambda}$) is measured by PILS system directly. The bulk absorption coefficient of BrC is calculated from Eq. 9:

$$Abs_{BrC+lensing\_\lambda} = Abs_{Total\_\lambda} - M_{BC} * MAC_{BC_{core_\lambda}} \quad (Eq. 9)$$

where the Abs_{Total_λ} is the total absorption coefficient measured by the PAS. MAC of the BC core is set to be 6.3 and 10.2 $m^2\ g^{-1}$, respectively, at 660 nm and 405 nm. It should be noted that both BrC and lensing contribute to the bulk absorption coefficient, and cannot be separated using this approach.

Then the plume integrated absorption and scattering were normalized (x/CO) by taking the ratio of background-subtracted absorption or scattering (Δx) to the background-subtracted CO mixing ratio (ΔCO) (Eq. 10), so that the changing of the normalized properties is not impacted by dilution of the plume with background air.

$$x/CO = \frac{\Delta x}{\Delta CO} \quad (Eq. 10)$$

2.7 Modified Combustion Efficiency (MCE)

The variation of burn condition (e.g., flaming vs. smoldering) and fuel type can cause a significant difference in BC emissions and changes in aerosol properties (Akagi et al., 2011; Andreae, 2019). Burn conditions can be estimated with the modified combustion efficiency (MCE), defined as Eq. 11:

$$MCE = \frac{\Delta CO_2}{\Delta CO + \Delta CO_2} \quad (Eq. 11)$$

where ΔCO_2 and ΔCO are the background-subtracted CO_2 and CO mixing ratio. The background of CO_2 and CO mixing ratio is obtained via the same process described in Section 2.3.

3 Results and Discussion

~~**Table 1: Average values and standard deviation of AMS factor, Mie factor at 660 nm and UHSAS factor for all the integrated plumes when using different particle density and WSOM:WSOC ratio. Unit of particle density is g cm^{-3}.**~~

Factor	Particle Density	WSOM:WSOC	Average	Standard Deviation
AMS factor	N/A	1.5	1.73	0.79
	N/A	1.6	1.63	0.74
	N/A	1.8	1.48	0.79
Mie factor at 660 nm	1.1	N/A	1.47	0.13
	1.4	N/A	1.47	0.13
	1.7	N/A	1.47	0.13
Mie factor at 405 nm	1.1	N/A	1.83	0.89
	1.4	N/A	1.83	0.89
	1.7	N/A	1.83	0.89
UHSAS factor	1.1	1.8	1.65	0.82
	1.4	1.6	2.36	1.17
	1.7	1.5	3.06	1.52

Figure 10 shows the time evolution of the fraction of non-BC absorption from BrC at 660 nm for the biomass burning plumes encountered during WE-CAN. Assuming a MAC of the BC core of 6.3 $m^2 g^{-1}$, BrC contributes roughly the same amount of absorption at 660 nm as lensing (62% UHSAS method, 46% AMS method). This means that 19% (based on the AMS) to 26% (based on the UHSAS) of the total absorption at 660 nm comes from BrC. When different particle density and WSOM:WSOC ratios are considered (top and bottom whiskers, as well as red and blue dashed lines), the fraction of non-BC absorption is 43-80% for the UHSAS approach and 41-49% for the AMS approach based on different OM:OC and density. While there is considerable variability between flights, a rule-of-thumb that roughly half of the non-BC absorption at red wavelengths is from absorbing organic material seems reasonable. To our knowledge, this is the first attempt to differentiate between lensing and absorbing organics in the red wavelengths. This approach assumes that water-insoluble BrC has the same refractive index as water-soluble BrC.

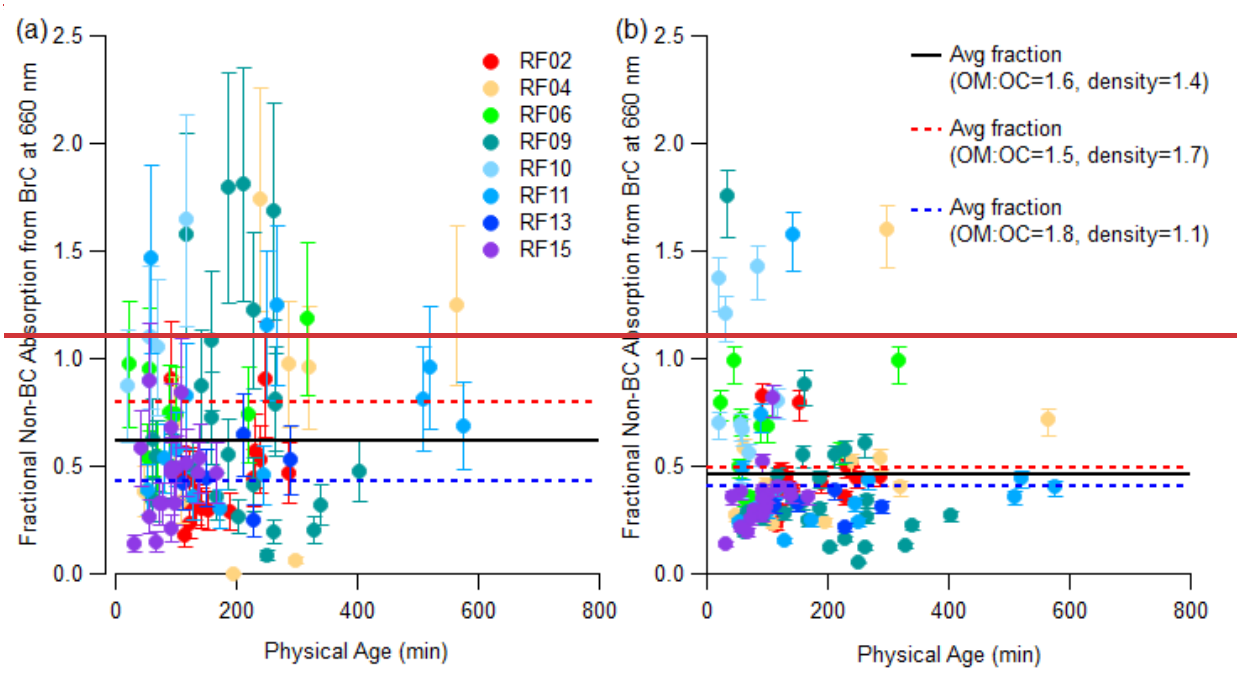

~~3.1.5 Aging of Water Soluble BrC at 660 nm~~

~~To further analyze the evolution of BrC at 660nm in wildfire emissions, the MAC of water soluble BrC at 660 nm (MAC_{ws_BrC660}) was calculated by taking the ratio of water soluble light absorption (β_{ws_BrC660}) and WSOC provided by the PILS (Eq. 4). Similar to MAC_{BC660}, MAC_{ws_BrC660} is relatively flat with physical age (Fig. 11a), with an average of 0.06 $m^2 g^{-1}$ and a standard deviation of 0.04 $m^2 g^{-1}$, but most of the plumes measured were less than 10 hours old. Interestingly, the fit lines for correlations with markers of chemical age suggest that MAC_{ws_BrC660} tends to be larger when these markers indicate a more oxidized plume (Fig. 11 b-e), which is distinct from what has been found in previous studies that BrC at shorter wavelengths decays with chemical age. The trend of increasing MAC_{ws_BrC660} is not clear in each flight and is only observed when properties are compared between fires. While the correlation coefficients are low, it can be stated that MAC_{ws_BrC660} is consistently larger in more oxidized plumes and there is not a decrease with increased oxidation or chemical aging. Given that all the observed smoke plumes were of similar physical ages, this again leads to the idea that these properties are the result of different emissions or fast chemistry that occurs before the plumes are first observed by the aircraft.~~

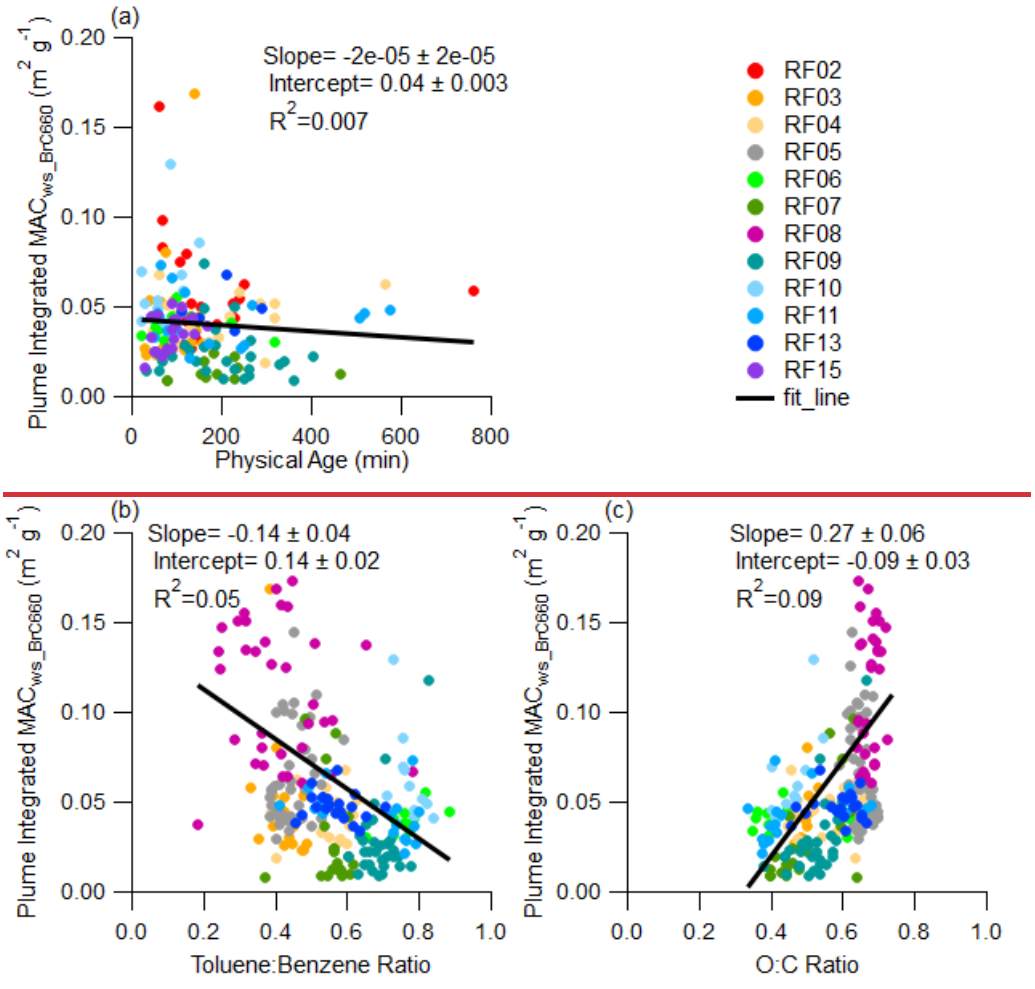

~~Figure 11: Plume integrated MAC_{ws_BrC660} variations with (a) Physical Age; (b) toluene:benzene ratio and (c) O:C ratio. RF05 and RF08 were measuring mixed aged smokes, during which the fire source cannot be identified, and therefore the physical age is unavailable for both flights.~~

~~The total MAC of BrC and lensing at 660 (measured by PAS, $MAC_{BrC+lensing\_660}$) is also compared with markers of chemical age (Fig. 12). $MAC_{BrC+lensing\_660}$ includes lensing, water soluble BrC, and water insoluble BrC. $MAC_{BrC+lensing\_660}$ also shows an increasing trend with chemical oxidation, which is consistent with the trend in MAC_{ws_BrC660}. Again, it is important to point out that while there is a weak trend for some individual flights, much of the trend of increasing MAC at 660 nm results from combining data from all the fires and much of the trend may be caused by emissions from different fires having different properties. Despite this, it is clear that plumes that appear chemically older by either the toluene:benzene ratio or the O:C ratio actually have larger MAC's in the red wavelength than plumes that appear chemically younger, a result that is exactly the opposite of the bleaching of BrC often seen at shorter wavelengths. In addition, these chemically "older" plumes have less BC, OA, and WSOC along with smaller bulk absorption. That is to say, when chemical markers indicate an "old" plume, the fire tends to emit darker (Fig. 11 and Fig. 12) organic aerosol, but less of it (Fig. 5 g-h and Fig. 6) resulting in less bulk absorption (Fig. 5e and 5f). The mean value of $MAC_{BrC+lensing\_660}$ is 0.11 $m^2 \cdot g^{-1}$ (with a standard deviation of 0.06), which is larger than the 0.06 average~~

of MAC_{ws_BrC660}, a result we have attributed to the lensing effect, but which could also partially be the result of water-insoluble BrC having a higher MAC than water-soluble BrC.

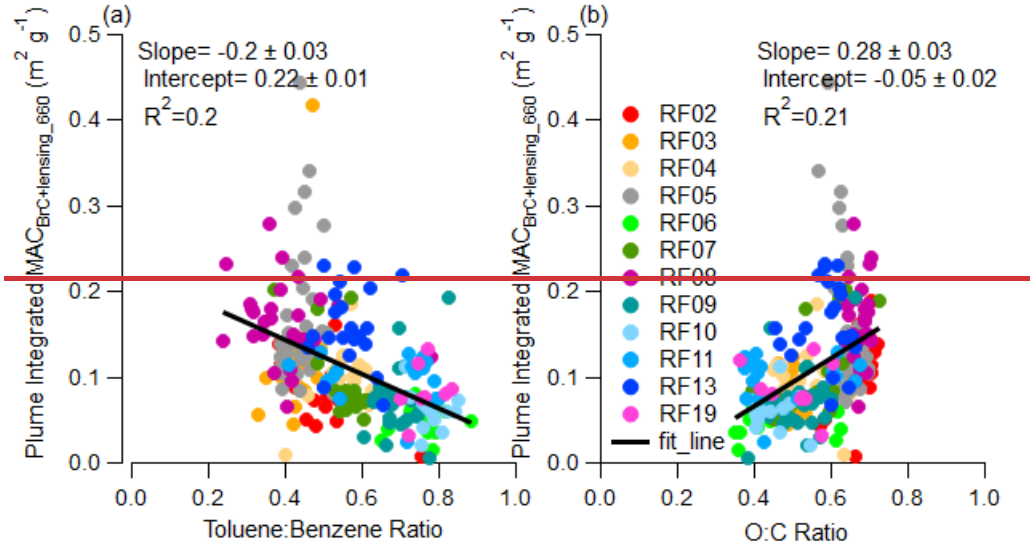

Figure 12: Plume integrated $MAC_{BrC+lensing\_660}$ variations with (a) toluene:benzene ratio and (b) O:C ratio.

The ratio of BC:OA has been shown to correlate to the optical properties of biomass burning aerosol (Pokhrel et al, 2016; Saleh et al., 2014). During WE-CAN, $MAC_{BrC+lensing\_660}$ showed an increasing trend with increasing BC:OA ratio (Fig. S6), which is similar to Saleh et al. (2014), who found that the imaginary part of the refractive index of OA at 550 nm increases with the BC:OA ratio. This consistency suggests that MAC of BrC at 550 nm and 660 nm have the same behavior in that BrC grows more absorbing as the BC:OA ratio increases.

3.2 Characteristics of BrC at 405 nm

3.2.1 Behavior of $MAC_{BrC+lensing\_405}$

Palm et al. (2020) utilized data from both WE-CAN and Monoterpene and Oxygenated aromatic Oxidation at Night and under LIGHTs (MOONLIGHT) campaigns and found that evaporated biomass burning POA is the dominant source of the biomass burning SOA in wildfire plumes, which happened in the first a few hours after emission. They also found that for those SOA that formed from oxidation, phenolic compounds contribute 29 ± 15% of BrC absorption at 405 nm. In this section, characteristics of BrC were also analyzed at 405 nm to understand if the behavior was similar or different to BrC decay at 660 nm. BrC at 405 nm was calculated in the same way that it was calculated at 660 nm, following Eq. 3, and therefore it also has a contribution from the lensing effect. Figure 13 shows the plume integrated $MAC_{BrC+lensing\_405}$ variations with (a) Physical Age and (b) MCE. Similar to 660 nm, $MAC_{BrC+lensing\_405}$ varies from fire to fire and no clear trend can be found with increasing physical age or MCE. Similar behavior was also observed in Western wildfires at 405 nm in FIREX-AQ (Zeng et al., 2022). The $MAC_{BrC+lensing\_405}$ varies from 0.08 $m^2 g^{-1}$ to 1.6 $m^2 g^{-1}$ with a mean value of 0.59 $m^2 g^{-1}$ and a standard deviation of 0.19. The largest values are from RF05, the flight through California, Oregon, and Idaho, where aged smoke from different fires was mixed. The large $MAC_{BrC+lensing\_405}$ in RF05 is related to relatively small OA (Fig. 5 g-h), which occurred when the

plane left the smoke-filled boundary layer during RF05. If we exclude $MAC_{BrC+lensing\_405}$ from RF05, the values range from 0.08 $m^2 \cdot g^{-1}$ to 1.09 $m^2 \cdot g^{-1}$, but still have a mean value of 0.59 $m^2 \cdot g^{-1}$ and a standard deviation of 0.15. Again, we note that this value includes the contribution of lensing. Despite this, our results lie in the same range as those measured without the contribution of lensing of 0.31 ± 0.09 $m^2 \cdot g^{-1}$ measured in CLARIFY-2017 (Taylor, 2020), 0.13–2.0 $m^2 \cdot g^{-1}$ measured in FIREX-AQ (Zeng et al., 2022), and 0.25–1.18 $m^2 \cdot g^{-1}$ measured in ORACLES (Zhang et al., 2022).

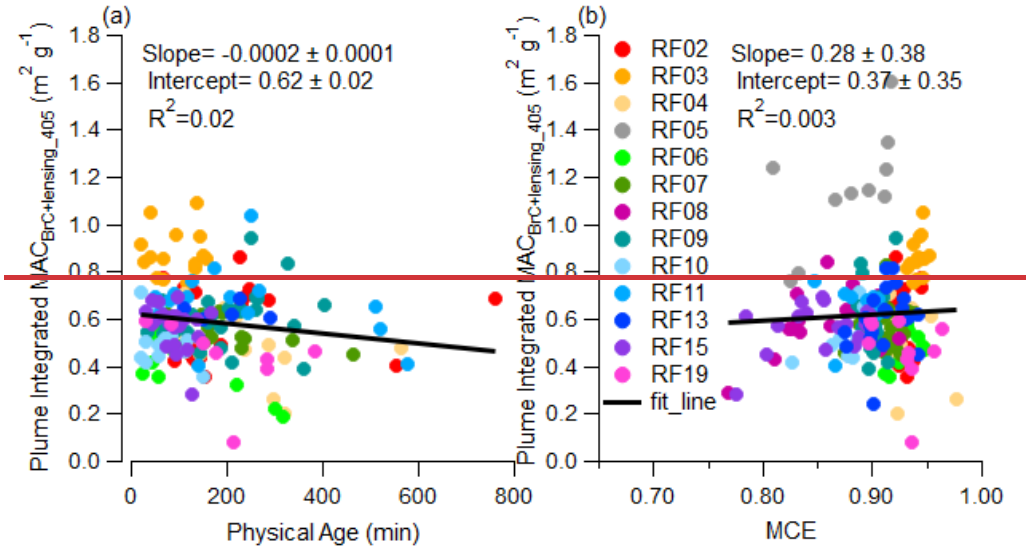

Figure 13: Plume integrated $MAC_{BrC+lensing\_405}$ variations with (a) Physical Age and (b) MCE

Figure 14 shows the behavior of brown carbon at 405 nm with markers of chemical aging. Very weak or non-trends are observed. If there is any trend, it is a slight increase in $MAC_{BrC+lensing\_405}$ with decreasing toluene:benzene ratio, which is consistent with the results for $MAC_{BrC+lensing\_660}$ (Fig. 12) and MAC_{ws_BrC660} (Fig. 11). The flat or slightly increasing trend with increasing oxidation shows that the decrease in total aerosol absorption with markers of chemical age is due to a decrease in OA (Fig. 5 g-h) because the BrC is actually darker in oxidized plumes at all wavelengths. It is important to remember that most of the trends observed in WE-CAN are caused by emissions from different fires versus variations within a fire, which tend to be quite small. Consistent results for the behavior of MAC_{BrC} at different wavelengths derived using different instruments (PAS and PILS) is further evidence that BrC decay does not occur in the WE-CAN dataset, or at least that plume integrated results cannot capture the BrC decay that might be occurring at the edges of the plume. While further research focused on the edge of the plumes, which often appear highly oxidized, is needed, this is beyond the scope of the current work. Despite this, it is the plume integrated results that are relevant for climate impacts and for comparison to model output, discussed in the following section.

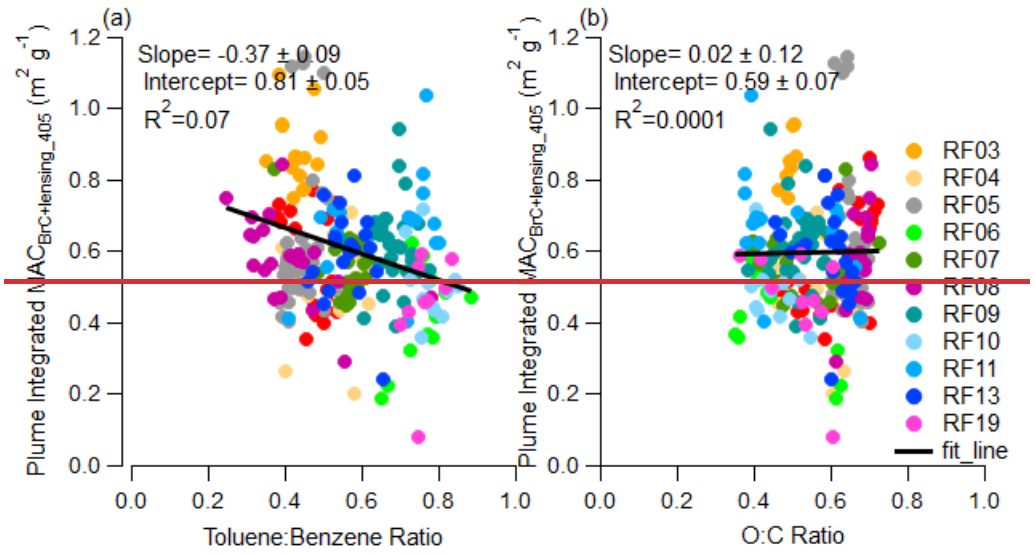

~~**Figure 14: Plume integrated $MAC_{BrC+lensing\_405}$ variations with (a) toluene:benzene ratio and (b) O:C ratio**~~

~~RF05 and RF08 are presented as case studies again to investigate the behavior of $MAC_{BrC+lensing\_405}$ in mixed plumes emitted from different fire sources. Figure 15 is similar to Fig. 8, but with $MAC_{BrC+lensing\_405}$ instead of MAC_{BC660}. For the case of RF05 (Fig. 15a) $MAC_{BrC+lensing\_405}$ varied from 0.36 $m^2 g^{-1}$ to 1.52 $m^2 g^{-1}$ with an average of 0.66 $m^2 g^{-1}$ and a standard deviation of 0.26 $m^2 g^{-1}$, the SSA_{450} averaged 0.94 with a standard deviation of 0.02, which is similar to SSA_{660}. The $MAC_{BrC+lensing\_405}$ is larger when CO mixing ratio is higher, but does not have a significant correlation with any other variables shown in Fig. 15. For the case of RF08 (Fig. 15b) $MAC_{BrC+lensing\_405}$ is more stable than in RF05, and varied from 0.25 $m^2 g^{-1}$ to 0.88 $m^2 g^{-1}$ with an average of 0.59 $m^2 g^{-1}$ and a standard deviation of 0.14 $m^2 g^{-1}$, the SSA_{450} average was 0.95 with a standard deviation of 0.01. The regional integrated $MAC_{BrC+lensing\_405}$ is even more stable with an average value of 0.59 $m^2 g^{-1}$ and a standard deviation of 0.07 $m^2 g^{-1}$.~~

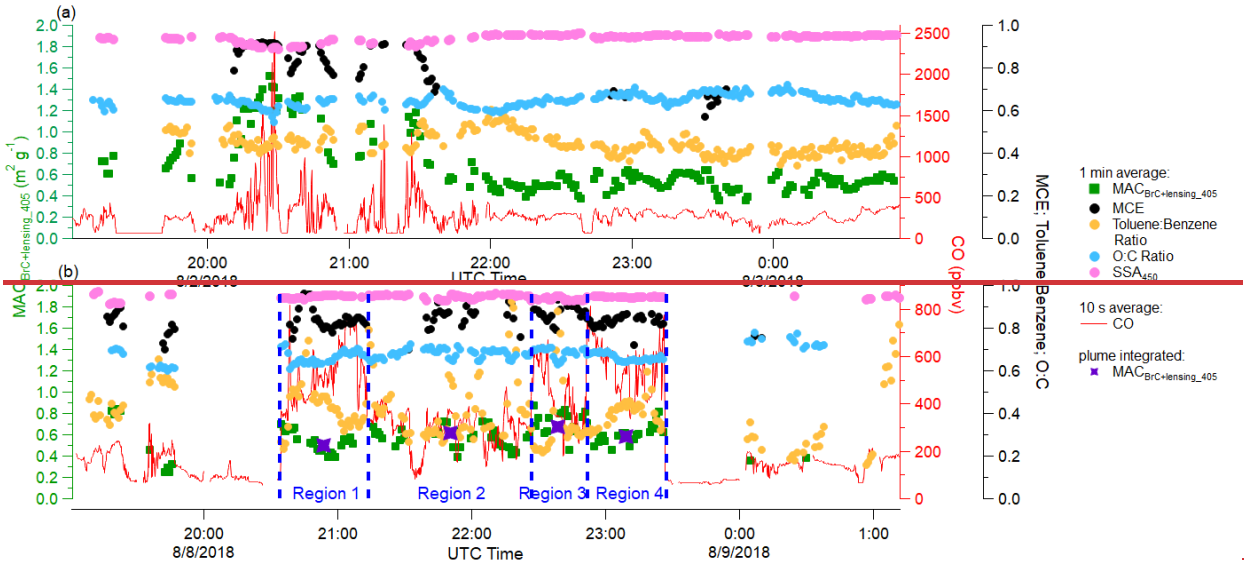

~~When comparing $MAC_{BrC+lensing\_405}$ with altitude and temperature (Fig. 16), it has the same behavior with MAC_{BC660} in that $MAC_{BrC+lensing\_405}$ stays relatively constant with both altitude and temperature. In addition, when $MAC_{BrC+lensing\_405}$ is plotted vs. ΔCO (not shown), no clear change in $MAC_{BrC+lensing\_405}$ is seen due to dilution. Therefore, both $MAC_{BrC+lensing\_405}$ and MAC_{BC660} do not appear to be affected by altitude or temperature during WE-CAN.~~

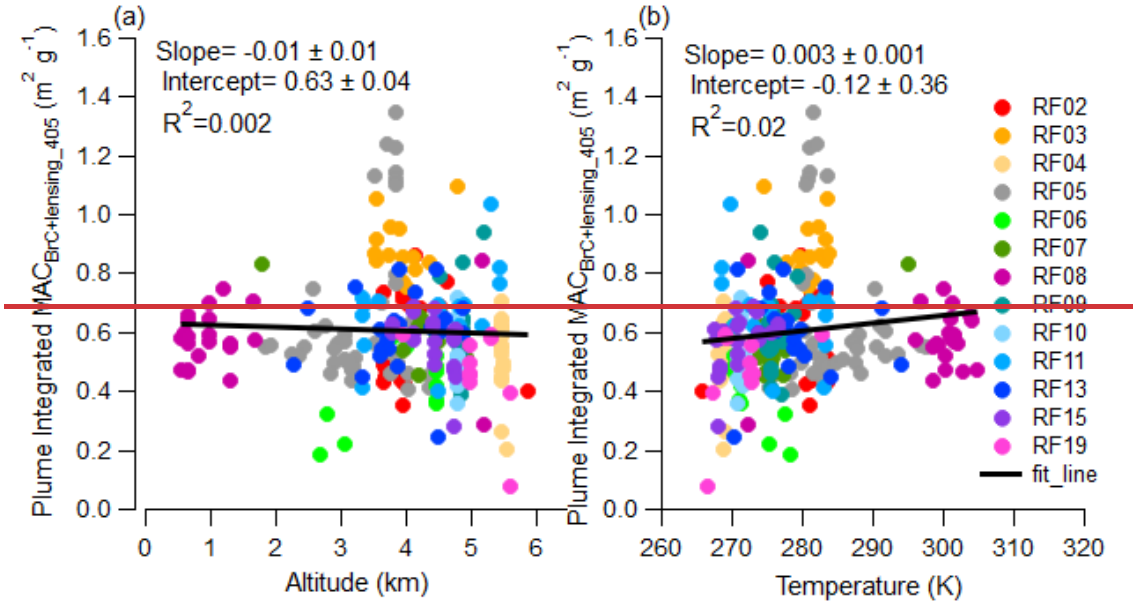

~~Figure 16: Plume integrated $MAC_{BrC+lensing\_405}$ variations with (a) Altitude and (b) Temperature~~

~~When comparing the relationship between $MAC_{BrC+lensing\_405}$ with the BC:OA ratio (Fig. S7), there is not a clear increasing trend, and the correlation is worse than that at 660 nm (Fig. S6). However, the increasing trend still exists in most individual flights (not in RF04 and RF10). The increasing trend is not as clear as in Saleh et al. (2014), most probably because the range of BC:OA ratios observed during WE-CAN (0.007–0.061) is much smaller than that (0.005–0.7) observed in Saleh's work. Even in their work, the increasing trend is not very clear if one only focuses on the region where the BC:OA ratio is less than 0.03. Also, the Saleh et al. results were obtained from laboratory burns and not wildfires, which might also cause a discrepancy.~~

~~3.2.2~~3.1 Comparison of WE-CAN ~~Results~~MAC_{BrC} to Modeling Studies

~~The BC:OA ratios measured during WE-CAN were utilized in the Saleh et al. parameterization (2014),~~ It is challenging for climate models to simulate absorption from BrC, especially because it is highly wavelength dependent and may change with chemical age (Liu et al., 2020). Recently the Saleh et al. (2014) parameterization has been implemented in models in an attempt to better parameterize the imaginary part of the BrC refractive index (Wang et al., 2018; Carter et al., 2021). To test how accurately the Saleh parameterization matched WE-CAN data, the BC:OA ratios measured during WE-CAN were input into the Saleh parameterization, which provides an imaginary part for the refractive index of BrC ($k_{BrC,\lambda}$) as a function of the BC:OA ratio. The ~~mean~~plume integrated BC:OA ratio for each plume was used in the parameterization, which gave an average k_{BrC} of 0.025, 0.013, 0.009, respectively, at 405 nm,

550 nm and 660nm. Mie theory (Bohren and Huffman, 1983) was then used to calculate the MAC for BrC~~, in which~~. To do the Mie calculations we assumed a real part of the refractive index of 1.7 for BrC (same as Saleh et al., 2014), ~~a~~used volume mean ~~diameter~~diameters measured for each plume, and ~~a~~used an organic density of 1.4 g cm^{-3}. Figure ~~1~~2 compares the observed $MAC_{BrC+lensing}$ (Eq. 4) and MAC_{ws_BrC} (Eq. 5) with the value calculated from the Saleh parameterization with inputs from WE-CAN. In both the observations and the parameterization, the MAC_{BrC} decreases as wavelength increases. However, the Saleh parameterization is always significantly larger than the observations. The MAC_{BrC} from the Saleh parameterization, which does not include lensing effects, is a factor of 3.4 and 2.8 larger than the observed $MAC_{BrC+lensing}$ at 405 nm and 660 nm, respectively. The range of BC:OA ratios during WE-CAN (0.007~0.061) is ~~much smaller than that~~on the very small end of the range (0.005~0.7) used in Saleh's work, and the parameterization failed to capture absorbing aerosol properties for this study. The discrepancy could also be partly because the data Saleh et al. used for their parameterization comes from controlled laboratory burns and not wildfires~~, or because of the sensitivity of MAC_{BrC} to density when using~~. It is worth noting that the Saleh parameterization~~. When we increase~~ of MAC_{BrC} is very sensitive to organic aerosol density. If particle density is increased from 1.4 g cm^{-3} to 1.7 g cm^{-3}, the Saleh parameterization median MAC_{BrC} decreases to 1.6 m^2 g^{-1} and 0.24 m^2 g^{-1}, respectively, at 405 nm and 660 nm (a factor of 2.8 and 2.3, respectively, compared to observed MAC_{BrC} at 405 nm and 660 nm). ~~This suggests~~The fact that the Saleh parameterization overestimates the absorption property of biomass aerosol especially for fresh emitted aerosols ~~and more~~suggests that different parameterizations ~~need to be developed.~~are needed for the Western U.S.. Carter et al. (2021) utilized the Saleh parameterization for BrC absorption in the GEOS-Chem model and also found that the Saleh model overestimated BrC absorption for WE-CAN. It was hypothesized that the overestimation was due to the lack of a bleaching process for BrC in the model and offset part of the overestimation by bringing in bleaching into the model. ~~However, our results show that the overestimation in the model is caused by an incorrect refractive index.~~

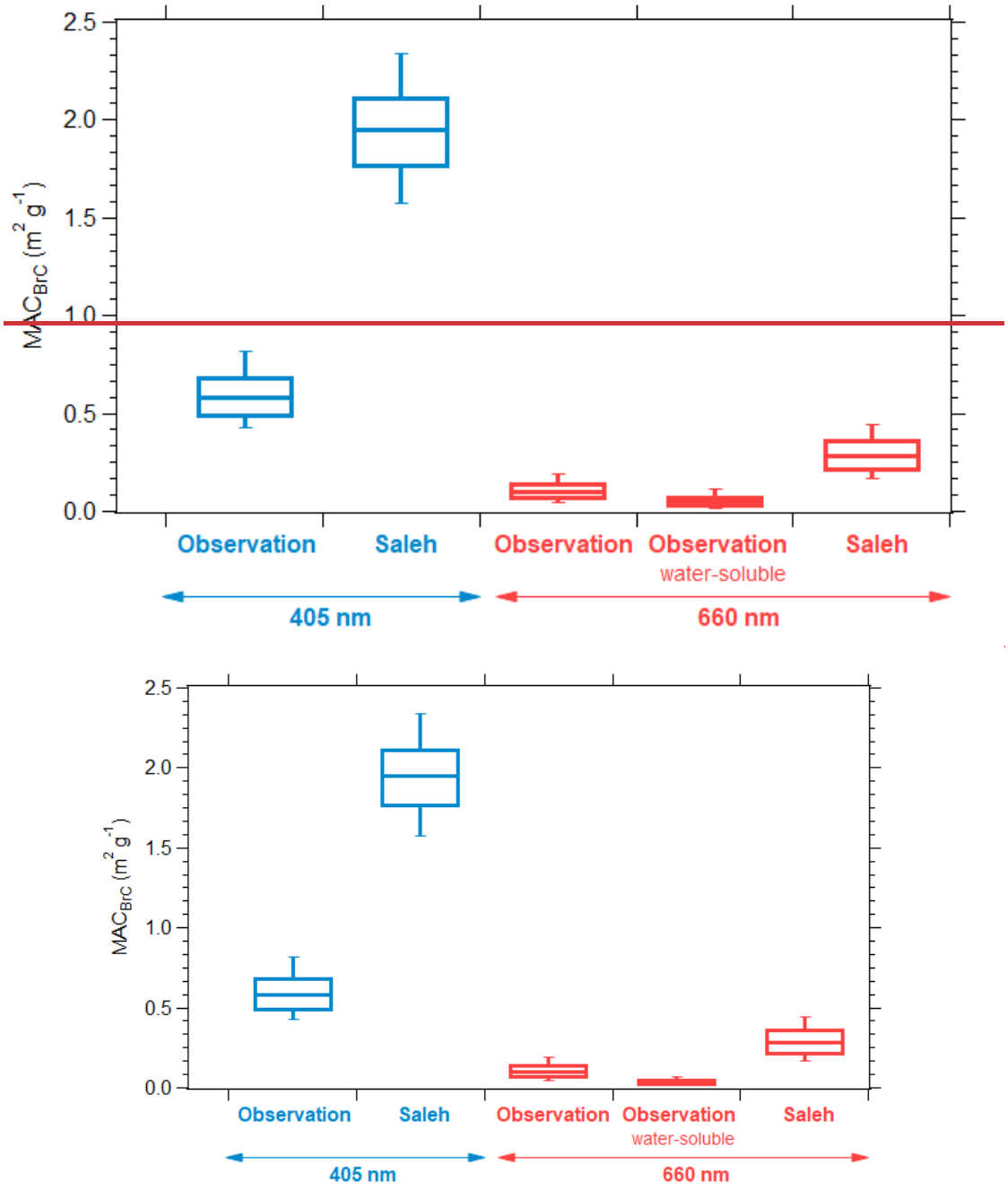

Figure ~~17~~2: Boxplot summary for observed and parameterized (Saleh) MAC_{BrC} at 405 nm (blue) and 660 nm (red). For each box, the central line represents the median, the top and bottom edges represent the 75th and 25th percentile, and the top and bottom whiskers represent the 90th and 10th percentile of the data.

3.2 Investigation of BrC Bleaching at Visible Wavelengths

A limited number of field measurements have shown BrC decay with chemical age (Forrister et al., 2015; Wang et al., 2016). Despite a relatively poor understanding of the mechanism of bleaching or whitening of BrC, this process has been implemented in numerous model simulations (Brown et al., 2018; Wang et al., 2018; Carter et al.,

2021). The definition of bleaching or whitening is unclear in previous literature, models tend to treat bleaching as the change of refractive index or decreasing of MAC (Brown et al., 2018; Wang et al., 2018; Carter et al., 2021), while observations or lab experiments mostly link bleaching to the decrease of absorption coefficient (Forrister et al., 2015; Palm et al., 2020; Zeng et al., 2022). It is important to distinguish between these two, because the decrease of absorption coefficient can also be caused by loss of absorbing organic material, which will also change the scattering coefficient and radiative forcing. Therefore, the MAC of BrC and the absorption coefficient of BrC at visible wavelengths were calculated and analyzed together with two chemical clocks (O:C and toluene:benzene ratio) and organic mass, to determine whether BrC bleached during the WE-CAN campaign, and whether the bleaching was caused by the less organic mass or the changing of refractive index. Because all large wildfire emissions are a mix of different regions that are burning slightly different fuels at different combustion efficiencies and because models treat regions, not individual fires, we identify relationships in this paper that hold true across all the flight data collected during WE-CAN. These types of broad correlations are much more useful than individual case studies yielding results that only hold true sometimes.

3.2.1 Consistency of The Mass Absorption Cross-Section of BrC at 405 nm

Palm et al. (2020) combined data from WE-CAN and the Monoterpene and Oxygenated aromatic Oxidation at Night and under LIGHTs (MOONLIGHT) chamber experiment and found that evaporated biomass-burning POA is the dominant source of biomass-burning SOA in wildfire plumes during the first a few hours after emission. They also found that of the SOA formed from oxidation, phenolic compounds contribute 29 ± 15% of BrC absorption at 405 nm. In this section, we analyze the characteristics of BrC at 405 nm to understand the average properties of BrC and to understand the balance of BrC formation versus bleaching during WE-CAN. The MAC of BrC is calculated following Eq. 4 and therefore it includes a contribution from the lensing effect. The MAC of water-soluble BrC is calculated following Eq. 5. Figure 3 shows the MAC of BrC at 405 nm versus the aerosol oxidation level (O:C ratio), while Fig. S2 is a similar plot that uses a simple photochemical clock, the gas-phase toluene:benzene ratio. The O:C ratio characterizes the oxidation state of OA and typically increases with photochemical age (Aiken et al., 2008), while the toluene:benzene ratio decreases with photochemical processing time since toluene is more reactive than benzene (Gouw et al., 2005). Both markers are two commonly used markers to indicate the chemical age of smoke, and they correlated well with each other during WE-CAN (Fig. S1).

The $MAC_{BrC+lensing\_405}$, varies from 0.08 $m^2\ g^{-1}$ to 1.6 $m^2\ g^{-1}$ with a mean value of 0.59 $m^2\ g^{-1}$ and a standard deviation of 0.19. The largest values are from RF05, the flight through California, Oregon, and Idaho, where aged smoke from different fires was mixed. The large $MAC_{BrC+lensing\_405}$ occurred when the aircraft left the smoke-filled boundary layer during RF05. If we exclude $MAC_{BrC+lensing\_405}$ from RF05, the values range from 0.08 $m^2\ g^{-1}$ to 1.09 $m^2\ g^{-1}$, but still have a mean value of 0.59 $m^2\ g^{-1}$ and a standard deviation of 0.15. Again, we note that this value includes the contribution of lensing. Despite this, our results lie in the same range as those measured without the contribution of lensing of 0.31 ± 0.09 $m^2\ g^{-1}$ measured in CLARIFY-2017 (Taylor, 2020), 0.13-2.0 $m^2\ g^{-1}$ measured in FIREX-AQ (Zeng et al., 2022), and 0.25-1.18 $m^2\ g^{-1}$ measured in ORACLES (Zhang et al., 2022). Very weak or non-trends are observed versus the chemical markers of aging (Fig. 3). If there is any trend, it is a slight increase in

MAC_{ws_BrC405} with O:C ratio with a poor correlation. A similar weak trend is also observed when compared MAC_{ws_BrC405} and $MAC_{BrC+lensing\_405}$ with the toluene:benzene ratio (Fig. S2). The flat or slightly increasing trend with increasing oxidation level and decreasing toluene:benzene suggests that the refractive index of BrC is not changing in a consistent way at 405 nm. It is important to remember that most of the trends observed in WE-CAN are caused by emissions from different fires versus variations within a single fire, which tend to be quite small. Only 2 flights shows a clear trend ($R^2 > 0.3$) for both MAC_{ws_BrC405} and $MAC_{BrC+lensing\_405}$ with increasing O:C ratio at the same time, and they are RF03 (R^2 of 0.85 and 0.85 with positive slope for MAC_{ws_BrC405} and $MAC_{BrC+lensing\_405}$), and RF06 (R^2 of 0.8 and 0.49 with negative slope for MAC_{ws_BrC405} and $MAC_{BrC+lensing\_405}$), where RF03 only measured a single fire (Taylor Creek fire).

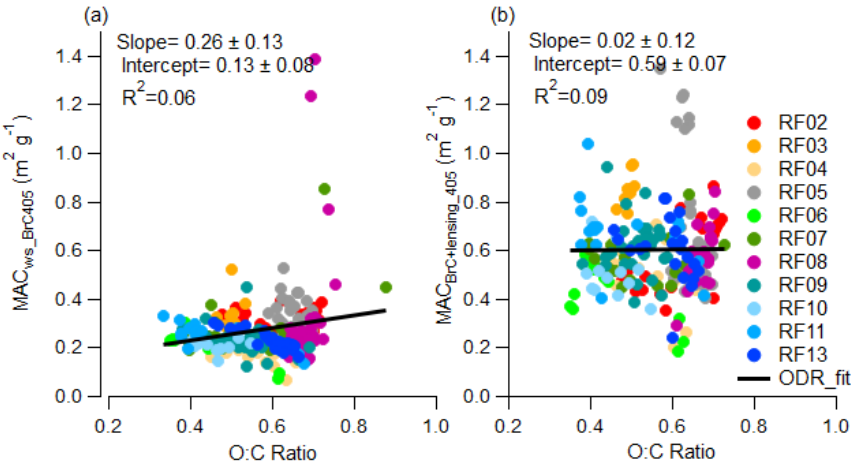

Figure 3: Plume integrated (a) MAC_{ws_BrC405} and (b)$MAC_{BrC+lensing\_405}$ variations with the organic aerosol O:C ratio

RF05 and RF08 were chosen as case studies, to observe the optical properties of highly aged aerosol to see if the optical properties of this aerosol were similar to those observed in the near-field plume sampling of individual fires at the longest chemical or physical age observed, which was roughly 6-24 hours of physical aging. RF08 was a flight through the Central Valley of California where aged smoke from multiple fires that had settled into the valley was measured while RF05 was a flight in which smoke from several California fires was observed in California, Oregon and Idaho roughly 300~600 miles from the fires (flightpaths are shown in Fig. 1). $MAC_{BrC+lensing\_405}$, CO mixing ratio, toluene:benzene ratio, and O:C ratio are displayed in Fig. 4a and 4b. The mixing ratio of CO is relatively low in these aged dilute smoke plumes vs. the plumes near the sources analyzed earlier. 1-minute averages of $MAC_{BrC+lensing\_405}$ are calculated to reduce noise and 1-minute-averages for toluene:benzene ratio and O:C ratio were calculated and all the negative values were removed. As shown in Fig. 4, the smallest toluene:benzene ratio is ~0.35 in RF05, and is ~0.16 in RF08, while the largest O:C ratio is ~0.7 in both RF05 and RF08, which indicates these two cases indeed captured plumes that appear chemically aged to similar extent to the other near-field flights where the smallest toluene:benzene ratio was 0.33 and the largest O:C ratio was 0.88 in near-fire measurements (Fig. 3 and Fig. S2).

In RF05 (Fig. 4a), the weighted average O:C ratio over the entire flight was 0.64, and the toluene:benzene ratio averaged 0.45 with a standard deviation of 0.05. $MAC_{BrC+lensing\_405}$ varied from 0.36 $m^2\ g^{-1}$ to 1.52 $m^2\ g^{-1}$ with an average of 0.66 $m^2\ g^{-1}$ and a standard deviation of 0.26 $m^2\ g^{-1}$. The plume that was measured in this flight was a mixture of different fire sources. Despite the much longer transit time and distance, overall these emissions, which were measured 300 to 600 miles away, have a very similar $MAC_{BrC+lensing\_405}$ to that of the near-source flights.

The RF08 (Fig. 4b) results are similar to RF05, even though these emissions were smoke of mixed aged from multiple fire sources in the Central Valley of California. The weighted average O:C ratio was 0.67 over the entire measurement, and average toluene:benzene ratio was 0.41 with a standard deviation of 0.15. $MAC_{BrC+lensing\_405}$ averaged 0.59 $m^2\ g^{-1}$ with a standard deviation is 0.14 $m^2\ g^{-1}$. There are several extreme values that exist in the dataset, probably because of time-alignment issues caused by variation in the dilution rate of the SP2 which cannot be totally eliminated from the 1-minute average. In addition, the smoke from RF08 (Fig. 4b) is split into four regions based on varying observed CO mixing ratios, and integrated $MAC_{BrC+lensing\_405}$ is calculated for each region (purple star marker). The regional edges are represented by blue dashed lines. Integrated $MAC_{BrC+lensing\_405}$ for all of these variable CO regions is relatively stable with an average value of 0.59 $m^2\ g^{-1}$ and a standard deviation of 0.07 $m^2\ g^{-1}$.

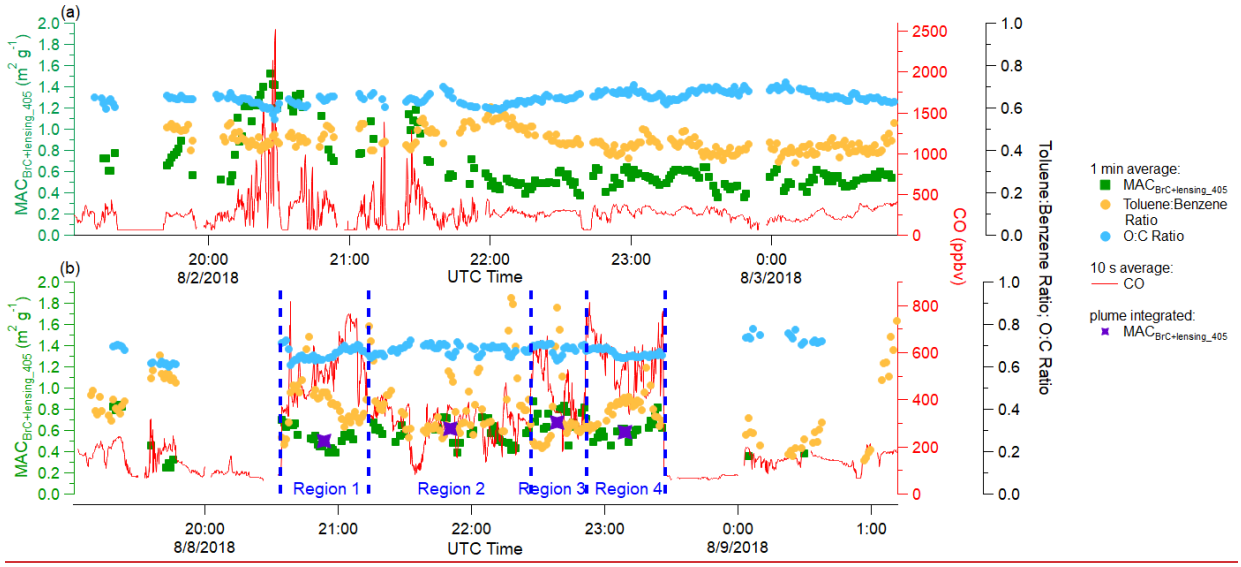

Figure 4: Time series of plume properties during (a) RF05 (measurements far from fire source), and (b) RF08 (Central Valley of California). Different square and round markers indicate 1 min averages of different variables as shown in the legend, and the red solid line represents 10 s averages of the mixing ratio of CO. Purple stars in RF08 indicate region integrated $MAC_{BrC+lensing\_405}$ (individual regions are separated based on the concentration of CO, and indicated by blue dashed lines).

3.2.2 Decrease in Absorption at 405 nm Observed with Markers of Chemical Oxidation

Although neither the $MAC_{BrC+lensing\_405}$ nor MAC_{ws_BrC405} decreases with O:C or Toluene:Benzene, Fig. 5 shows that BrC bleaching is observed in terms of decreased total absorption. Figure 5a and 5c show the behavior of BrC absorption at 405 nm with markers of the aerosol oxidation level (O:C) and photochemistry (toluene:benzene). The absorption coefficient of BrC shown in Fig. 5 is calculated by Eq. 9-10, which cannot separate the absorption

caused by the BrC and lensing effect. To confirm that observed trends are not the result of changing lensing, the absorption coefficient of water-soluble BrC measured by the PILS, which does not include lensing effects, is also compared in Fig. 6a and 6c. The average water-soluble BrC absorption at 405 nm (Abs_{ws_BrC405}, 0.02 Mm^{-1} $ppbv^{-1}$) is only 20% of the total absorption from BrC plus lensing ($Abs_{BrC+lensing\_405}$, 0.11 Mm^{-1} $ppbv^{-1}$). However, $Abs_{BrC+lensing\_405}$ and Abs_{ws_BrC405} both decrease with increasing O:C (R^2 = 0.65 and R^2 = 0.3, respectively for $Abs_{BrC+lensing\_405}$ and Abs_{ws_BrC405}) and decreasing toluene:benzene ratio, which suggest a similar level of decreasing BrC absorption for all the fires observed in WE-CAN from numerous locations in the western U.S.. This relationship holds despite differences in fuel type, burn conditions, meteorology, etc. between all of these fires. The observed trends are mostly due to the decreasing of both total OA mass (Fig. 5b and 5d) and WSOC (Fig. 6b and 6d) with the increasing O:C ratio (R^2 = 0.8 and R^2 = 0.4, respectively for OA and WSOC) and decreasing toluene:benzene ratio (R^2 = 0.64 and R^2 = 0.44, respectively for OA and WSOC). Overall, the organic aerosol O:C ratio better predicts BrC evolution than toluene:benzene ratio, probably because it is a particle-phase property rather than a gas-phase one. Again, it is important to clarify if BrC "bleaching" is caused by decreasing BrC absorption coefficient or decreasing of BrC refractive index (or MAC). In this study, decreasing MAC_{BrC} is not observed, rather the BrC absorption coefficient decreases significantly with the the simple O:C and Toluene:Benzene chemical clocks due to loss of OA mass. Less OA mass also causes decrease in bulk scattering coefficient (Fig. S3), leading to a very different net radiative effect than reducing MAC_{BrC}.

It is important to recall that we aimed to find general trends that hold for all fires in the western U.S., and the above trend is significant when all fires are grouped together, although the trend is, in fact, not robust in each flight and is rather due to variations between the fire plumes rather than variation within a single fire plume. Figure 7 shows the correlation between normalized OA and chemical age for each fire source. It demonstrates that different fires show different relationships and that OA does not always decrease with oxidation level/chemical aging within a single fire (Kiwah fire and Rabbitfoot fire), though increasing O:C ratio does correlate well (R^2 > 0.3) with decreasing OA mass in 7 fires (with R^2 of 0.94 for Taylor Creek fire, 0.87 for Carr fire, 0.86 for Beaver Creek fire, 0.8 for Coal Hollow fire, 0.76 for Bear Trap fire, 0.35 for Sharps fire, and 0.31 for Sugarloaf fire). Toluene:benzene ratio didn't track OA as good as O:C ratio, and decreasing toluene:benzene ratio correlates well (R^2 > 0.3) with decreasing OA mass in 3 fires (with R^2 of 0.87 for Rabbitfoot fire, 0.85 for Coal Hollow fire, and 0.84 for Bear Trap fire).

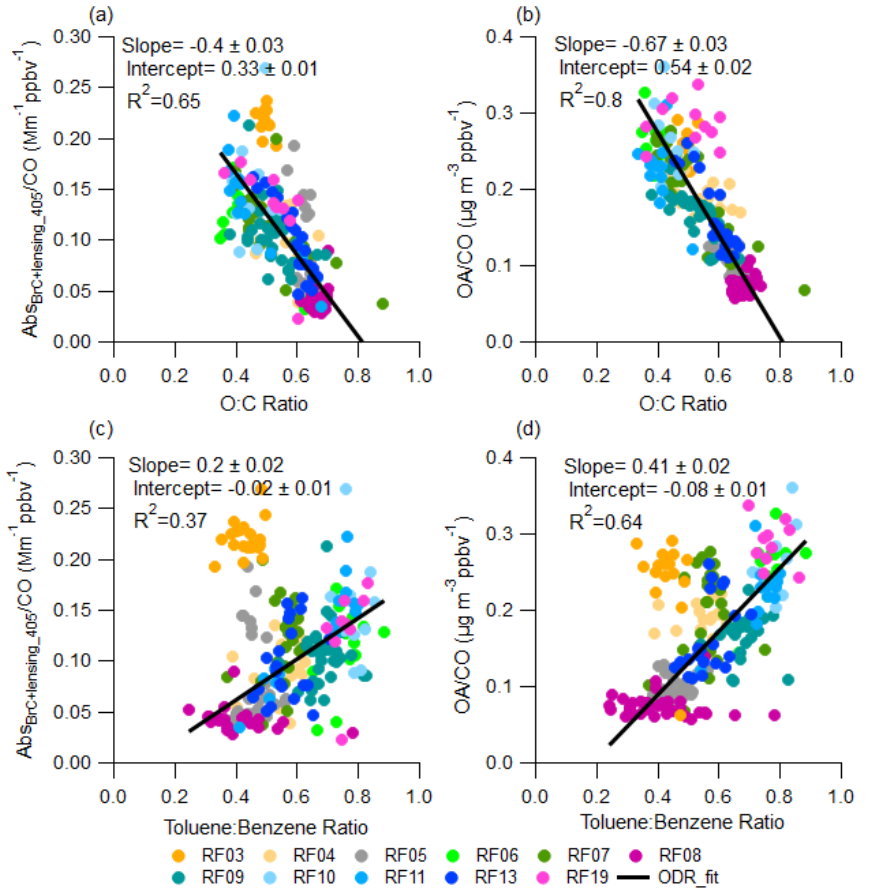

Figure 5: Plume integrated normalized $Abs_{BrC+lensing\_405}$, and OA variation with chemical age. Top panels show (a) plume integrated normalized $Abs_{BrC+lensing\_405}$, and (b) plume integrated normalized OA variation with O:C ratio. Bottom panels show (c) plume integrated normalized $Abs_{BrC+lensing\_405}$, and (d) plume integrated normalized OA variation with toluene:benzene ratio. Data from RF03 was excluded from the ODR fit with toluene:benzene ratio, because RF03 sampled the injection of fresh smoke into the free troposphere, where gas species reacted more rapidly than particles and toluene:benzene ratio failed to keep track of aerosol evolution.

808

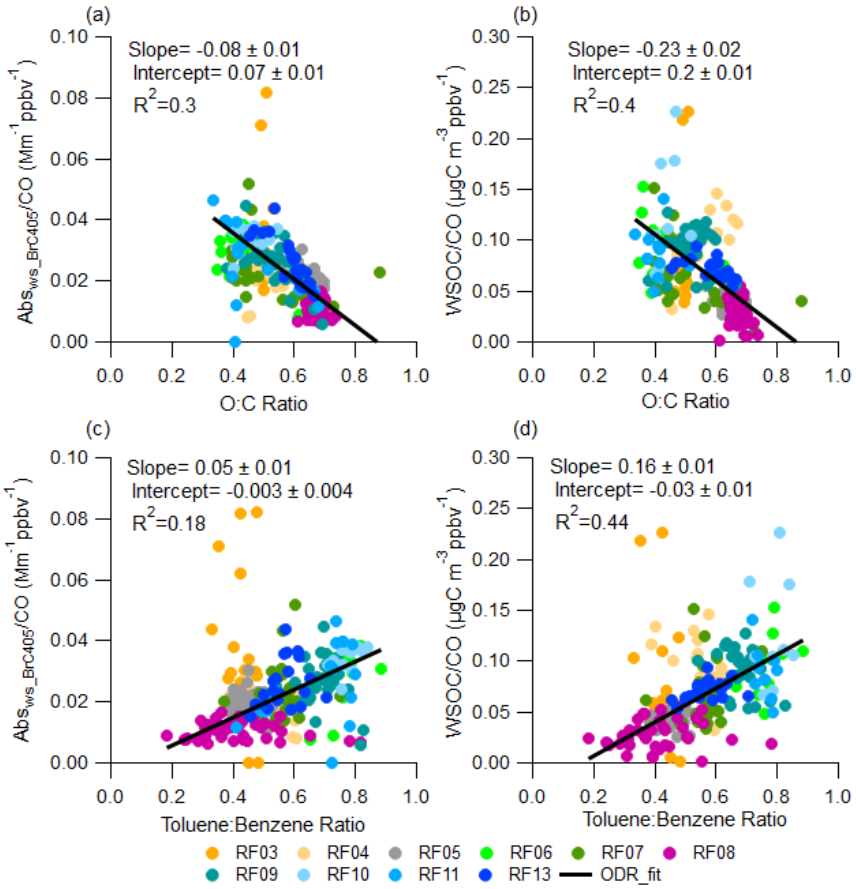

Figure 6: Similar to Fig. 5, but with plume integrated normalized Abs_{ws_BrC405}, from PILS in (a) and (c), and WSOC in (b) and (d)

809

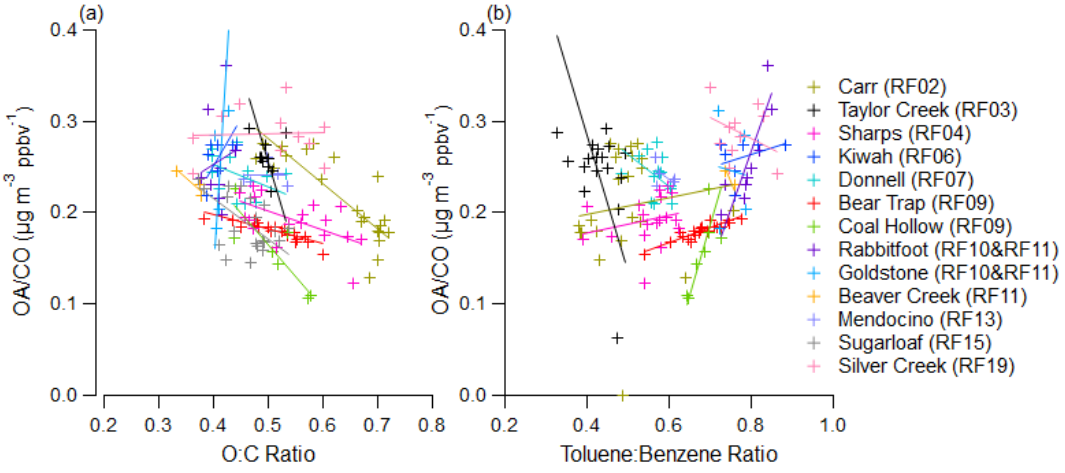

Figure 7: Plume integrated normalized OA variation with (a) O:C ratio and (b) toluene:benzene ratio. Different colors were used to distinguish plumes from different fire sources. Plumes from uncertain fire sources (especially plumes from RF05, RF08) were not included in this plot.

810

No trend is observed in CO normalized OA mass with plume physical age (Fig. S4), which is consistent with the result from Garofalo et al. (2019) in that no net OA mass change was observed in individual plumes during WE-CAN when they are characterized by physical age, although more data from additional fires were included in the current work. Plume-integrated CO-normalized OA also shows weak or no trend with altitude and temperature (Fig. S5). However, we note that the smallest OA:CO was captured in the plumes (RF08) that have highest temperature (~305 K), and larger OA:CO tends to be observed in the colder plumes (RF19). More studies are needed to determine how much OA is evaporated in high temperature plumes because the WE-CAN dataset does not capture enough variation of temperature within plumes to make a robust conclusion. No clear trend was found between $MAC_{BrC+lensing\_405}$ and physical age or MCE (Fig. S6). Similar behavior was also observed in Western wildfires at 405 nm in FIREX-AQ (Zeng et al., 2022). Part of the reason is that for most fires, we only captured the first few hours (< 15 h), and MCE do not have a robust capability to predict biomass burning particle properties (McClure et al., 2020). No trend is found between $MAC_{BrC+lensing\_405}$ and altitude or temperature (Fig. S7). The trend with BC:OA ratio (Fig. S8) is not as clear as in Saleh et al. (2014), most probably because the range of BC:OA ratios observed during WE-CAN (0.007~0.061) is much smaller than that (0.005~0.7) observed in Saleh's work. Even in their work, the increasing trend is not very clear if one only focuses on the region where the BC:OA ratio is less than 0.03. Also, the Saleh et al. (2014) results were obtained from laboratory burns and not wildfires, which might also cause a discrepancy.

3.2.3 Mass Absorption Cross-Section and Optical Properties of BrC at 660 nm

BrC is defined as OA that has strong absorption at UV and shorter visible portions of the spectrum and has been historically considered to be almost transparent near the red wavelengths (Andreae and Gelencsér, 2006; Bahadur et al., 2012; Liu et al., 2020). However, during WE-CAN, we were able to quantify Abs_{ws_BrC660} with the PILS instrument. We know that absorption observed in the PILS at 660 nm is not BC because BC is insoluble and will be removed by the 0.2 μm filter in the instrument. Next, we investigate the behavior of BrC absorption at 660 nm to see if BrC has a similar behavior at the long versus short ends of the visible spectrum.

Figure 8 shows the behavior of brown carbon at 660 nm vs. the O:C ratio. Similar to 405 nm, no bleaching in terms of decreased MAC is observed at 660 nm. If there is any trend, it is increasing MAC_{ws_BrC660} and $MAC_{BrC+lensing\_660}$ with organic aerosol O:C ratio. Similar trends are observed, though with lower correlation, versus the toluene:benzene ratio (Fig. S9). The mean value of $MAC_{BrC+lensing\_660}$ is 0.11 $m^2\ g^{-1}$ (with a standard deviation of 0.06), which is much larger than the 0.03 average of MAC_{ws_BrC660}, a result we have attributed to the lensing effect, but which could also partially be the result of water-insoluble BrC having a higher MAC than water-soluble BrC.

These results for the behavior of MAC_{BrC} at different wavelengths derived using different instruments (PAS and PILS) is further evidence that MAC_{BrC} does not decrease with physical or chemical age in the WE-CAN dataset. At a minimum, the plume integrated results, which represent total optical properties relevant to climate models, do not capture any MAC_{BrC} decay that might be occurring at the edges of the plume.

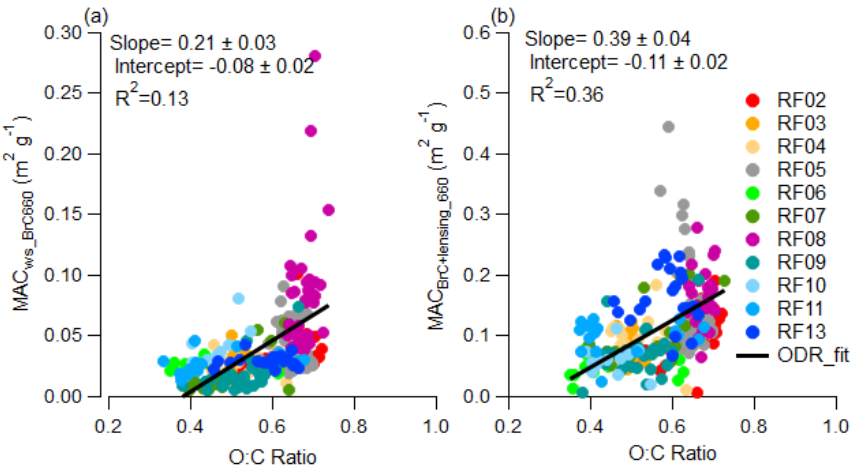

Figure 8: Plume integrated (a) MAC_{ws_BrC660} and (b)$MAC_{BrC+lensing\_660}$ variations with O:C ratio

Similar to our analysis at 405 nm, RF05 and RF08 are presented as case studies to investigate the behavior of $MAC_{BrC+lensing\_660}$ in aged plumes emitted from different fire sources. Figure 9 is similar to Fig. 4, but with $MAC_{BrC+lensing\_660}$ instead of $MAC_{BrC+lensing\_405}$. For the case of RF05 (Fig. 9a) $MAC_{BrC+lensing\_660}$ varied from 0.04 m^2 g^{-1} to 0.40 m^2 g^{-1} with an average of 0.15 m^2 g^{-1} and a standard deviation of 0.07 m^2 g^{-1}. The $MAC_{BrC+lensing\_660}$ tends to be larger when CO mixing ratio is higher, but does not have a significant correlation with any marker of oxidation level or photochemistry shown in Fig. 9. For the case of RF08 (Fig. 9b) $MAC_{BrC+lensing\_660}$ is more stable than in RF05, and varied from 0.04 m^2 g^{-1} to 0.37 m^2 g^{-1} with an average of 0.18 m^2 g^{-1} and a standard deviation of 0.06 m^2 g^{-1}. The regional integrated $MAC_{BrC+lensing\_660}$ is even more stable with an average value of 0.16 m^2 g^{-1} and a standard deviation of 0.01 m^2 g^{-1}. Similar to the results at 405 nm, we observe that the MAC in these very aged plumes is very similar to the average MAC observed in the near field.

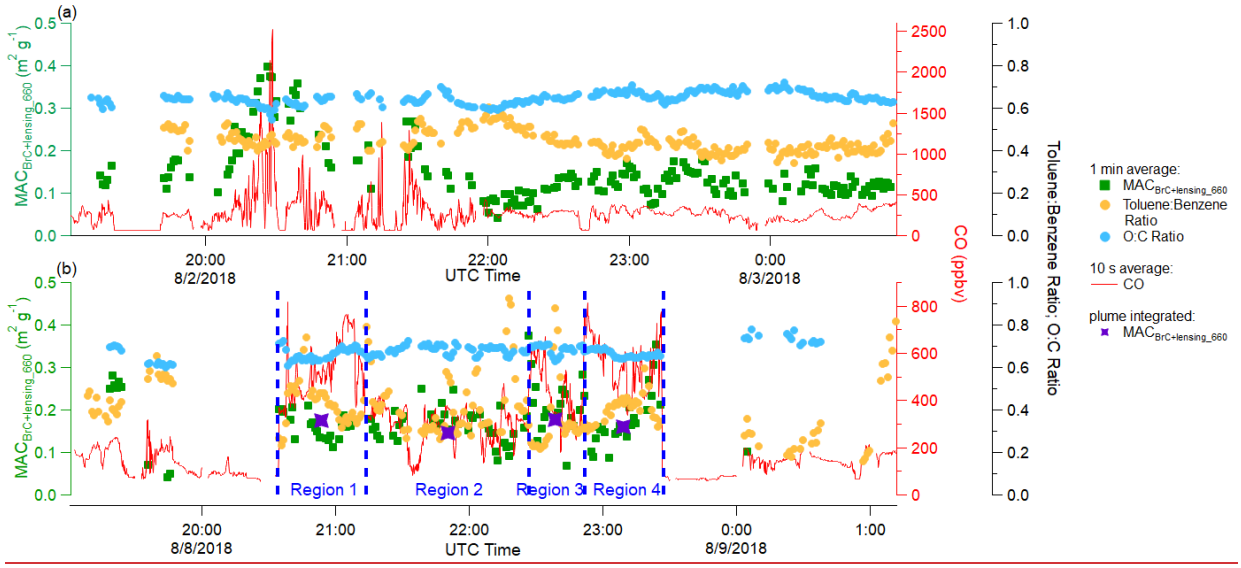

Figure 9: Time series of plume properties during (a) RF05, and (b) RF08(Central Valley of California). Different square and round markers indicate 1 min averages of different variables as shown in the legend, and the red solid line represents 10 s averages of the mixing ratio of CO. Purple stars in RF08 indicate region integrated $MAC_{BrC+lensing\_660}$ (individual regions are separated based on the concentration of CO, and indicated by blue dashed lines).

Normalized $Abs_{BrC+lensing\_660}$ and total scattering coefficient at 660 nm (Fig. S10), as well as normalized Abs_{ws_BrC660} (Fig. S11) were also investigated to see if they decreased with markers of chemical age similar to the results seen at 405 nm. However, the correlation between these BrC optical properties with O:C ratio or toluene:benzene ratio at 660 nm is much weaker and flatter than they are at 405 nm. Perhaps this is because BrC absorption is very small at 660 nm, and a large uncertainty is brought in from the assumptions required for calculation of this property and instrumental uncertainties. The average normalized $Abs_{BrC+lensing\_660}$ is 0.02 Mm^{-1} $ppbv^{-1}$, which is 5 times lower than the absorption at 405 nm; while the average normalized Abs_{ws_BrC660} is a order of magnitude lower than Abs_{ws_BrC405}. The $MAC_{BrC+lensing\_660}$ (Fig. S12) shows better correlation with BC:OA ratio than $MAC_{BrC+lensing\_405}$, though the increasing trend is still not as significant as Saleh et al. (2014) due to a much smaller BC:OA ratio during WE-CAN.

3.3 Relative Importance of BrC vs. the Lensing Effect at 660 nm

Plume integrated MAC_{BC} at 660 nm (MAC_{BC660}) from the 13 WE-CAN research flights with clear plume transects of biomass burning plumes are shown in Fig. 10. The MAC_{BC660} discussed in this section is calculated from Eq. 3, and has contributions from absorption from the BC core, the BrC shell, and the lensing effect. Again, even fire plumes from individually named fires are usually a mix of many different burning conditions, and it is hard to identify the exact source in most wildfire smoke measurements, especially for well mixed plumes. Therefore flight-to-flight data is analyzed because each flight covered a region, and an overall behavior of absorbing aerosol from wildfire can be provided. MAC_{BC660} varies between different flights with RF03 having the highest average MAC_{BC660} of 12.9 m^2 g^{-1}, and RF10 having the lowest average MAC_{BC660} of 8.6 m^2 g^{-1}. Even in highly aged plumes with emissions mixed from multiple fires (RF05 and RF08), the MAC_{BC660} is similar in magnitude and consistency with an average of 11.3

± 1.8 m^2 g^{-1}. The average of all plume-integrated MAC_{BC660} is 10.9 m^2 g^{-1}, with a standard deviation of 2.1 m^2 g^{-1}. This result is similar to some other recent airborne measurements. Subramanian et al. (2010) reported a MAC_{BC660} of 10.9 ± 2.1 m^2 g^{-1} using a SP2 and PSAP operated during the MILAGRO campaign, which included airborne measurements of biomass burning over Mexico. Similarly, Zhang et al. (2017) estimated a MAC_{BC660} of 10 m^2 g^{-1} utilizing both SP2 and PSAP deployed on the NASA DC-8 research aircraft for the DC3 campaign, which measured the upper tropospheric BC over the central U.S. Taylor et al. (2020) calculated a MAC_{BC655} of 12 ± 2 $m^2 g^{-1}$ for biomass burning emissions from Africa over the southeast Atlantic Ocean, using airborne measurements from a SP2 and PAS in the CLARIFY-2017 campaign.

These results are encouragingly similar given the breadth of measurement techniques (PSAP is filter-based whereas PAS is a direct measurement), geographic regions (Continental U.S. for DC3, Mexico for MILAGRO, African outflow for CLARIFY) and altitude in the atmosphere (all were airborne campaigns covering a range of altitudes). If we apply 6.3 m^2 g^{-1} as the MAC of a BC core at 660 nm (Bond and Bergstrom, 2006; Subramanian et al., 2010), then the average absorption enhancement for the entire WE-CAN campaign is 1.7. This means the absorption of coated BC is 1.7 times higher than bare BC at 660 nm, which is somewhat close to the factor of ~2 reported by laboratory experiments (Schnaiter et al., 2005; Peng et al., 2016), larger than some field measurements (Cappa et al., 2012&2019; Healy et al., 2015), but close to 1.85 ± 0.45 measured by Taylor et al. (2020) in African biomass burning plumes. The similarity to the Taylor et al. (2020) result suggests global similarities in the MAC_{BC660} from aerosol emitted from wildfires.

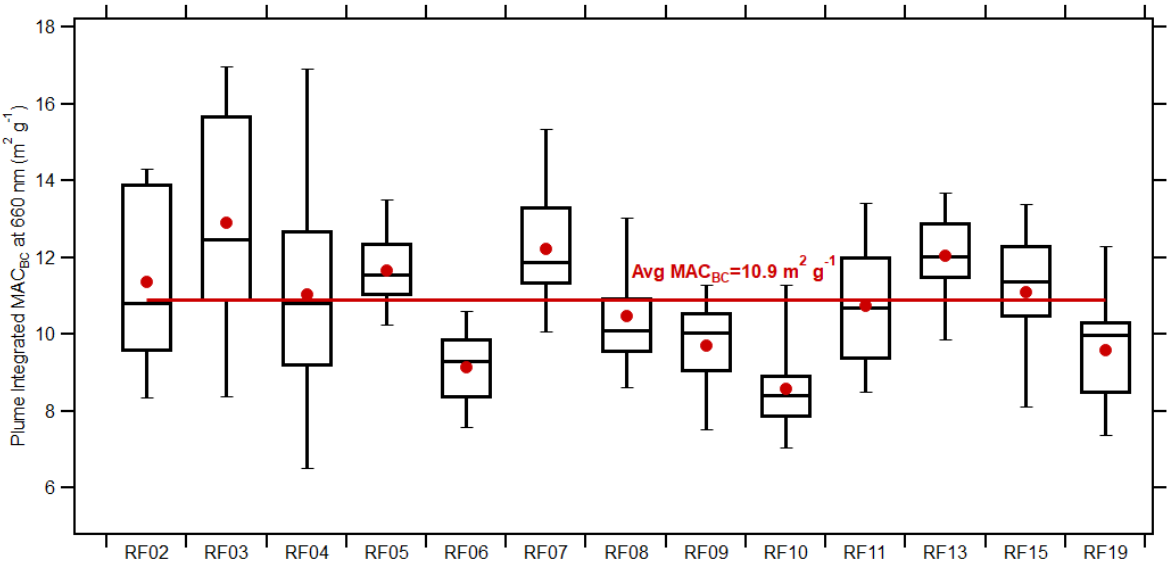

Figure 10: Box plots of plume integrated MAC_{BC660} for each flight. On each box the central line represents the median, the top and bottom ~~edge represents 75% and 25%, the top and bottom whisker represents 90% and 10%,~~edges represent the 75th and 25th percentile, and the top and bottom whiskers represent the 90th and 10th percentile of the data. The red dot shows the average, and the red line indicates the average value for all plume integrated MAC_{BC660}.

MAC_{BC660} is also compared with the physical age and MCE (Fig. S13), the O:C and toluene:benzene chemical clocks (Fig. S14), and the altitude, temperature and dilution (ΔCO) (Fig. S15). However, no clear trend is be found in these comparisons.

The average absorption enhancement of 1.7 at 660 nm in this study indicates that, on average, 41% of total absorption at 660 nm is caused by lensing and absorbing organics, instead of BC itself. Figure 11 shows the fraction of non-BC absorption from BrC at 660 nm for the biomass burning plumes encountered during WE-CAN using Eq. 6-8 with OM calculated from the AMS. The figure is plotted versus plume physical age to allow visualization of the variability, though there is no clear trend with physical age other than perhaps a decrease in variability with increasing physical age. Figure S16 shows a similar result by using OM calculated from the UHSAS. More details on the calculation and the AMS vs. UHSAS methods are explained in section 2.5. Assuming a MAC of the BC core of 6.3 $m^2 g^{-1}$, BrC contributes roughly the same amount of absorption at 660 nm as lensing (46% from the AMS method, 62% from theUHSAS method). This means that 19% (AMS method) to 26% (UHSAS method) of the total absorption at 660 nm comes from BrC. When different particle density and WSOM:WSOC ratios are considered (top and bottom whiskers, as well as red and blue dashed lines), the fraction of non-BC absorption is 41-49% for the AMS approach (Fig. 11) and 43-80% for the UHSAS approach (Fig. S16) based on different OM:OC and density. The UHSAS approach shows larger uncertainty because it's sensitive to the particle density when calculating particulate mass (Table S1). While there is considerable variability between flights, a rule of thumb that roughly half of the non-BC absorption at red wavelengths is from absorbing organic material seems reasonable. To the best of our knowledge, this is the first observation-based attempt to differentiate between lensing and absorbing organics in the red wavelengths. This approach assumes that water insoluble BrC has the same refractive index as water soluble BrC.

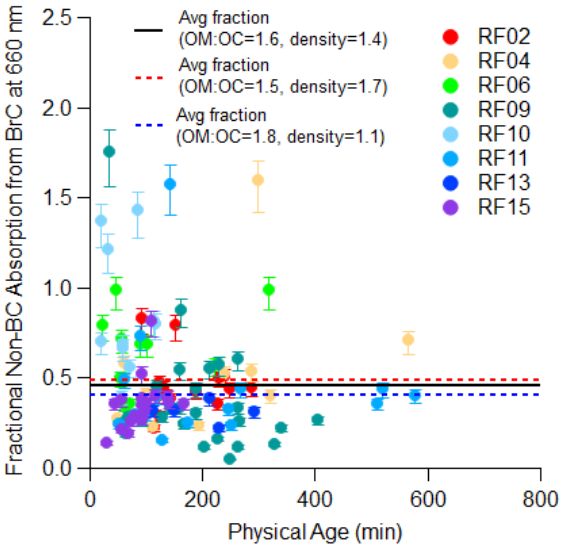

Figure 11: Time evolution of the fraction of non-BC absorption from BrC at 660 nm with AMS and Mie factor. Markers were calculated using a density of 1.4 g cm^{-3} and WSOM:WSOC ratio of 1.6. The top whiskers represent sensitive test values using a density of 1.7 g cm^{-3} and WSOM:WSOC ratio of 1.5, while the bottom whiskers represent sensitive test values using a density of 1.1 g cm^{-3} and WSOM:WSOC ratio of 1.8. The averaged fraction of non-BC absorption from BrC from all the plumes are shown in black solid lines, while the range of this result from sensitivity tests are shown in red and blue dashed lines.

4 Conclusion

~~**4 Conclusion**~~

In this study, we presented results that ~~help use~~enable a better ~~understand~~understanding of the ability of ~~wildfire~~ aerosol emissions from wildfires to absorb visible light and how those properties change after emission. We presented mass absorption coefficients (MAC) for ~~black~~BC and ~~brown carbon~~BrC from Western United States wildfires measured during the WE-CAN campaign at both short and long visible wavelengths (MAC_{BC660}, $MAC_{BrC+lensing\_660}$, MAC_{ws_BrC660}, $MAC_{BrC+lensing\_405}$). ~~We also investigated single scattering albedo (SSA), total scattering and total absorption at 660. We observed that the mass absorption coefficient of black carbon stayed relatively constant across all plumes measured and at all physical ages (ages up to 15 hours observed), with an averaged MAC_{BC660} of 10.9 ± 2.1 m^2 g^{-1} (average ± standard deviation). This average showed no variation with altitude or temperature, and we saw no evidence that MAC_{BC660} is correlated to MCE.~~ We also investigated the bulk absorption coefficient for BrC and bulk scattering coefficient for total aerosol at both short and long visible wavelengths. General trends that held for all the fire sources are derived, which should be valid throughout the western U.S. given the ~~Even in highly aged plumes with emissions mixed from multiple fires (RF05 and RF08), the MAC_{BC660} is similar in magnitude and consistency with an average of 11.3 ± 1.8 m^2 g^{-1}. Both the fact that this MAC is significantly larger than the MAC for uncoated BC (often cited to be ~ 6.3 m^2 g^{-1}) and the fact that the MAC remains relatively constant~~

~~across different fires and different plume ages are key insights that can improve models of aerosol optical properties in wildfire emissions.~~

~~We find that total organic aerosol (OA) and water soluble organic carbon (WSOC) are strongly correlated with markers of chemical age. OA and WSOC (both normalized to CO) decrease with decreasing toluene:benzene ratio or increasing O:C ratio. However, this phenomenon is observed in variations between different fire sources rather than during the aging of individual fire plumes. We interpret this variability to mean the fires either had different emission ratios of toluene:benzene and O:C or the smoke underwent rapid secondary chemistry prior to the first plume pass in WE-CAN. Regardless, the correlations are relatively strong (R^2 of 0.24 to 0.71) and provide a potential link between chemical markers and total organic aerosol amounts across a~~ wide ~~range of fires. While OA and WSOC decrease with decreasing toluene:benzene or increasing O:A, MAC_{BC660} actually shows a weak increasing trend with these same markers of aging, showing that while the total amount of organic aerosol is decreasing, the ability of the organic to absorb per mass is staying relatively constant, or even increasing.~~ variety of emissions used to develop them.

~~Through a novel use of PILS data, we find that BrC contributes 41–80% of non-BC absorption at 660 nm (assuming 6.3 $m^2 g^{-1}$ as the MAC of BC core at 660 nm). BrC contributes, on average, 26% of total absorption, but the absorption cross section of water-soluble BrC is relatively small at 660 nm, with a MAC_{ws_BrC660} of 0.06 ± 0.04 $m^2 g^{-1}$, which does not change with physical age. The average $MAC_{BrC+lensing\_660}$ derived from the PAS (which includes both brown carbon absorption and lensing of black carbon) is 0.11 ± 0.06 $m^2 g^{-1}$.~~

~~In the blue visible wavelengths where brown carbon is more often thought about, $MAC_{BrC+lensing\_405}$ is 0.59 ± 0.19 $m^2 g^{-1}$ and shows little variation with physical age or MCE. There are weak increasing trends in all the MAC_{BrC} data we obtained (MAC_{ws_BrC660}, $MAC_{BrC+lensing\_660}$ and $MAC_{BrC+lensing\_405}$) with markers of chemical age (toluene:benzene, O:C), while bulk absorption of total aerosol decreases with these same markers of chemical age. In highly aged plumes from multiple fires (RF05 and RF08), the $MAC_{BrC+lensing\_405}$ has an average value of 0.63 ± 0.2 $m^2 g^{-1}$, suggesting that brown carbon remains significantly absorbing even at relatively longer ages.~~

By utilizing a common parameterization for BrC refractive index from Saleh et al. (2014), with measured inputs for the BC:OA ratio and particle size, we calculated the theoretical MAC_{BrC660} and MAC_{BrC405}, and they were 2.3~3.4 times larger than the measured $MAC_{BrC+lensing}$ during WE-CAN. While this discrepancy has been resolved previously by implementing bleaching into model schemes, we show that this is probably the incorrect explanation given the MAC of ~~brown carbon is actually higher~~BrC either remains constant or slightly increases when chemical markers (O:C, toluene:benzene) suggest more oxidation~~.~~ has occurred. We suggest a ~~new BrC~~different parameterization of the refractive index is needed to represent wildfire optical properties in the Western United States rather than using bleaching to decrease the mass absorption cross section (MAC) of the Saleh parameterization. We also note that there needs to be better terminology to distinguish between decreasing absorption caused by losses of organic aerosol mass versus decreasing absorption caused by changes in the ~~mass absorption cross section (MAC) of the aerosol. Finally, these results are based on the plume integration method, which might neglect aerosol decay at the edge of the plume where oxidation and evaporation are more rapid compared to the center of the plume. While this effect may be important for studying mechanisms of smoke evolution, it does not affect mean properties, which are what ultimately affect climate and are comparable to modeling results~~MAC of the aerosol.

In the blue visible wavelengths, where BrC is more often thought about, $MAC_{BrC+lensing\_405}$ is 0.59 ± 0.19 m^2 g^{-1} and shows little variation with physical age, MCE, altitude, temperature or BC:OA ratio. There isn't any decreasing trends in all the MAC_{BrC} data we obtained (MAC_{ws_BrC405}, $MAC_{BrC+lensing\_405}$, MAC_{ws_BrC660}, and $MAC_{BrC+lensing\_660}$) with markers of chemical age (toluene:benzene, O:C), but bulk absorption of BrC does decrease with these same markers. In highly aged plumes from multiple fires (RF05 and RF08), the $MAC_{BrC+lensing\_405}$ has an average value of 0.63 ± 0.2 m^2 g^{-1}, suggesting that brown carbon remains significantly absorbing even at relatively longer ages.

We find that total organic aerosol (OA) and water-soluble organic carbon (WSOC) are strongly correlated with chemical markers of oxidative age. OA and WSOC (both normalized to CO) decrease with decreasing toluene:benzene ratio and increasing O:C ratio. However, this phenomenon is only clearly observed when data from all the observed fires is included rather than during the aging of individual fire plumes. This could mean that the fires either had different emission ratios of toluene:benzene and O:C or the smoke underwent rapid secondary chemistry prior to the first plume pass in WE-CAN. Regardless, the correlations are fairly robust (R^2 of 0.4 to 0.8) given the many variables (MCE, fuel type, etc.) that are changing in the dataset and provide a potential link between chemical markers and total organic aerosol amounts across a wide range of fires. While OA and WSOC decrease with decreasing toluene:benzene or increasing O:C, MAC_{BrC} actually shows a weak increasing trend with these same markers of aging, showing that while the total amount of organic aerosol is decreasing, the ability of the organic to absorb per mass is staying relatively constant, or even increasing. We also found that the bulk scattering coefficient (normalized to CO) decreases with decreasing toluene:benzene ratio or increasing O:C ratio due to less OA being present, which leads to a very different net radiative effect than that which results from just changing the refractive index of BrC.

In the red visible wavelengths, where BrC is often less noticed, we observed that the MAC of BC stayed relatively constant across all plumes measured and at all physical ages (ages up to 15 hours observed), with an averaged MAC_{BC660} of 10.9 ± 2.1 m^2 g^{-1} (average ± standard deviation), which includes the contribution from both lensing effect and absorbing organics. This average showed no clear trends with altitude or temperature, and we saw no evidence that MAC_{BC660} is correlated to MCE. Even in highly aged plumes with emissions mixed from multiple fires (RF05 and RF08), the MAC_{BC660} is similar in magnitude to the near-source plumes with an average of 11.3 ± 1.8 m^2 g^{-1}. Both the fact that this MAC is significantly larger than the MAC for uncoated BC (often cited to be ~ 6.3 m^2 g^{-1}) and the fact that the MAC remains relatively constant across different fires and different plume ages are key insights that can improve models of aerosol optical properties in wildfire emissions.

Through a novel use of PILS data, we find that BrC contributes 41-80% of non-BC absorption at 660 nm (assuming 6.3 m^2 g^{-1} as the MAC of BC core at 660 nm). BrC contributes, on average, 26% of total absorption, but the absorption cross section of water-soluble BrC is relatively small at 660 nm, with a MAC_{ws_BrC660} of 0.03 ± 0.02 m^2 g^{-1}, which does not change with physical age, and no trend with MCE is observed. The average $MAC_{BrC+lensing\_660}$ derived from the PAS (which includes both brown carbon absorption and lensing of black carbon) is 0.11 ± 0.06 m^2 g^{-1}.

Data Availability

The WE-CAN data can be found at http://data.eol.ucar.edu/master_lists/generated/we-can/.

The DOI for each data set used in this work are:

PAS and CAPS PM_{SSA}: https://doi.org/10.26023/K8P0-X4T3-TN06

PILS1: https://doi.org/10.26023/9H07-MD9K-430D and https://doi.org/10.26023/CRHY-NDT9-C30V

PILS2: https://doi.org/10.26023/7TAN-TZMD-680Y

SP2: https://doi.org/10.26023/P8R2-RAB6-N814

UHSAS: https://doi.org/10.26023/BZ4F-EAC4-290W

PTR-ToF-MS: https://doi.org/10.26023/K9F4-2CNH-EQ0W

HR-AMS: https://doi.org/10.26023/MM2Y-ZGFQ-RB0B

Picarro: https://doi.org/10.26023/NNYM-Z18J-PX0Q

miniQCL: https://doi.org/10.26023/Q888-WZRD-B70F

Author Contributions

SMM designed the project. YS wrote the paper. YS, RPP, APS, EJTL, LAG, DKF, WP, LH, DWT, TC, EVF, and SMM collected and analyzed data.

Competing Interests

The authors declare that they have no conflict of interest.

Acknowledgements

The 2018 WE-CAN field campaign was supported by the U.S. National Science Foundation through grants AGS-1650493 (U of Wyoming), AGS-1650786 (Colorado State U), AGS-1650275 (U of Montana), AGS-1650288 (U of Colorado at Boulder), and the National Oceanic and Atmospheric Administration (Award # NA17OAR4310010, Colorado State U). This material is based upon study supported by the National Center for Atmospheric Research, which is a major facility sponsored by the National Science Foundation under Cooperative Agreement no. 1852977. The authors acknowledge support from AGS-1650493 for YS, SMM and RPP, AGS-1650786 for APS and EJTL, AGS-2144896 for LH and WP, AGS-1650288 for DWT, NOAA Climate Program Office's Atmospheric Chemistry, Carbon Cycle, and Climate program (Grant NA17OAR4310010) for DKF and LAG.

We sincerely thank Ernie Lewis for his work implementing Mie theory into Igor code.

References

Aiken, A. C., Decarlo, P. F., Kroll, J. H., Worsnop, D. R., Huffman, J. A., Docherty, K. S., et al. (2008). O/C and OM/OC ratios of primary, secondary, and ambient organic aerosols with high-resolution time-of-flight aerosol

mass spectrometry. *Environmental Science and Technology*, *42*(12), 4478–4485. https://doi.org/10.1021/es703009q

Akagi, S. K., Yokelson, R. J., Wiedinmyer, C., Alvarado, M. J., Reid, J. S., Karl, T., et al. (2011). Emission factors for open and domestic biomass burning for use in atmospheric models. *Atmospheric Chemistry and Physics*, *11*(9), 4039–4072. https://doi.org/10.5194/acp-11-4039-2011

Andreae, M. O. (2019). Emission of trace gases and aerosols from biomass burning – An updated assessment. *Atmospheric Chemistry and Physics Discussions*, 1–27. https://doi.org/10.5194/acp-2019-303

Andreae, M. O., & Gelencsér, A. (2006). Black carbon or brown carbon? The nature of light-absorbing carbonaceous aerosols. *Atmospheric Chemistry and Physics*, *6*, 3131–3148. https://doi.org/10.5194/acp-6-3131-2006

Bahadur, R., Praveen, P. S., Xu, Y., & Ramanathan, V. (2012). Solar absorption by elemental and brown carbon determined from spectral observations. *Proceedings of the National Academy of Sciences*, *109*(43), 17366–17371. https://doi.org/10.1073/pnas.1205910109

Bohren, C. F., and Huffman, D. R. (1983). Absorption and Scattering of Light by Small Particles. John Wiley & Sons, Inc.

Bond, T. C., & Bergstrom, R. W. (2006). Light absorption by carbonaceous particles: An investigative review. *Aerosol Science and Technology*, *40*(1), 27–67. https://doi.org/10.1080/02786820500421521

Bond, T. C., Habib, G., & Bergstrom, R. W. (2006). Limitations in the enhancement of visible light absorption due to mixing state. *Journal of Geophysical Research Atmospheres*, *111*(20), 1–13. https://doi.org/10.1029/2006JD007315

Bond, T. C., Doherty, S. J., Fahey, D. W., Forster, P. M., Berntsen, T., Deangelo, B. J., et al. (2013). Bounding the role of black carbon in the climate system: A scientific assessment. *Journal of Geophysical Research Atmospheres*, *118*(11), 5380–5552. https://doi.org/10.1002/jgrd.50171

Brown, H., Liu, X., Feng, Y., Jiang, Y., Wu, M., Lu, Z., et al. (2018). Radiative effect and climate impacts of brown carbon with the Community Atmosphere Model (CAM5). *Atmospheric Chemistry and Physics*, 18(24), 17745–17768. https://doi.org/10.5194/acp-18-17745-2018

Brown, H., Liu, X., Pokhrel, R., Murphy, S., Lu, Z., Saleh, R., et al. (2021). Biomass burning aerosols in most climate models are too absorbing. *Nature Communications*, 12(1), 1–15. https://doi.org/10.1038/s41467-020-20482-9

Burke, M., Driscoll, A., Heft-Neal, S., Xue, J., Burney, J., & Wara, M. (2021). The changing risk and burden of wildfire in the United States. *Proceedings of the National Academy of Sciences of the United States of America*, 118(2), 1–6. https://doi.org/10.1073/PNAS.2011048118

Canagaratna, M. R., Jimenez, J. L., Kroll, J. H., Chen, Q., Kessler, S. H., Massoli, P., et al. (2015). Elemental ratio measurements of organic compounds using aerosol mass spectrometry : characterization , improved calibration , and implications. *Atmospheric Chemistry and Physics*, *15*(1), 253–272. https://doi.org/10.5194/acp-15-253-2015

Cappa, C. D., Onasch, T. B., Massoli, P., Worsnop, D. R., Bates, T. S., Cross, E. S., et al. (2012). Radiative absorption enhancements due to the mixing state of atmospheric black carbon. *Science*, *337*(6098), 1078–1081. https://doi.org/10.1126/science.1223447

Cappa, C. D., Zhang, X., Russell, L. M., Collier, S., Lee, A. K. Y., Chen, C. L., et al. (2019). Light Absorption by Ambient Black and Brown Carbon and its Dependence on Black Carbon Coating State for Two California, USA, Cities in Winter and Summer. *Journal of Geophysical Research: Atmospheres*, *124*(3), 1550–1577. https://doi.org/10.1029/2018JD029501

Carter, T. S., Heald, C. L., Cappa, C. D., Kroll, J. H., Campos, T. L., Coe, H., et al. (2021). Investigating Carbonaceous Aerosol and its Absorption Properties from Fires in the western US (WE-CAN) and southern Africa (ORACLES and CLARIFY). *Journal of Geophysical Research Atmospheres*, 1–28. https://doi.org/10.1029/2021JD034984

Chen, M., Sun, Z., Davis, J. M., Liu, Y. A., Corr, C. A., & Gao, W. (2019). Improving the mean and uncertainty of ultraviolet multi-filter rotating shadowband radiometer in situ calibration factors: Utilizing Gaussian process regression with a new method to estimate dynamic input uncertainty. *Atmospheric Measurement Techniques*, *12*(2), 935–953. https://doi.org/10.5194/amt-12-935-2019

Cho, C., Kim, S. W., Lee, M., Lim, S., Fang, W., Gustafsson, Ö., et al. (2019). Observation-based estimates of the mass absorption cross-section of black and brown carbon and their contribution to aerosol light absorption in East Asia. *Atmospheric Environment*, *212*(November 2018), 65–74. https://doi.org/10.1016/j.atmosenv.2019.05.024

~~Chylek, P., Lee, J. E., Romonosky, D. E., Gallo, F., Lou, S., Shrivastava, M., et al. (2019). Mie Scattering Captures Observed Optical Properties of Ambient Biomass Burning Plumes Assuming Uniform Black, Brown, and Organic Carbon Mixtures. *Journal of Geophysical Research: Atmospheres*, *124*(21), 11406–11427. https://doi.org/10.1029/2019JD031224~~

Craig, L., Moharreri, A., Schanot, A., Rogers, D. C., Dhaniyala, S., Craig, L., et al. (2013a). Characterizations of Cloud Droplet Shatter Artifacts in Two Airborne Aerosol Inlets. *Aerosol Science and Technology*, *47:6*, 662–671. https://doi.org/10.1080/02786826.2013.780648

Craig, L., Schanot, A., Moharreri, A., Rogers, D. C., & Dhaniyala, S. (2013b). Design and Sampling Characteristics of a New Airborne Aerosol Inlet for Aerosol Measurements in Clouds. *Journal of Atmospheric and Oceanic Technology*, *30*, 1123–1135. https://doi.org/10.1175/JTECH-D-12-00168.1

Craig, L., Moharreri, A., Rogers, D. C., Anderson, B., & Dhaniyala, S. (2014). Aircraft-Based Aerosol Sampling in Clouds : Performance Characterization of Flow-Restriction Aerosol Inlets. *Journal of Atmospheric and Oceanic Technology*, *31*, 2512–2521. https://doi.org/10.1175/JTECH-D-14-00022.1

Duarte, R. M. B. O., Freire, S. M. S. C., & Duarte, A. C. (2015). Investigating the water-soluble organic functionality of urban aerosols using two-dimensional correlation of solid-state 13C NMR and FTIR spectral data. *Atmospheric Environment*, *116*, 245–252. https://doi.org/10.1016/j.atmosenv.2015.06.043

Duarte, R. M. B. O., Piñeiro-Iglesias, M., López-Mahía, P., Muniategui-Lorenzo, S., Moreda-Piñeiro, J., Silva, A. M. S., & Duarte, A. C. (2019). Comparative study of atmospheric water-soluble organic aerosols composition in contrasting suburban environments in the Iberian Peninsula Coast. *Science of the Total Environment*, *648*, 430–441. https://doi.org/10.1016/j.scitotenv.2018.08.171

Eatough, D. J., Wadsworth, A., Eatough, D. A., Crawford, J. W., Hansen, L. D., & Lewis, E. A. (1993). A multiple-system, multi-channel diffusion denuder sampler for the determination of fine-particulate organic material in

the atmosphere. *Atmospheric Environment Part A, General Topics*, *27*(8), 1213–1219. https://doi.org/10.1016/0960-1686(93)90247-V

Finessi, E., Decesari, S., Paglione, M., Giulianelli, L., Carbone, C., Gilardoni, S., et al. (2012). Determination of the biogenic secondary organic aerosol fraction in the boreal forest by NMR spectroscopy. *Atmospheric Chemistry and Physics*, *12*(2), 941–959. https://doi.org/10.5194/acp-12-941-2012

Ford, B., Val Martin, M., Zelasky, S. E., Fischer, E. V., Anenberg, S. C., Heald, C. L., & Pierce, J. R. (2018). Future Fire Impacts on Smoke Concentrations, Visibility, and Health in the Contiguous United States. *GeoHealth*, 2(8), 229–247. https://doi.org/10.1029/2018gh000144

Forrister, Haviland; Liu, Jiumeng; Scheuer, Eric; Dibb, Jack; Ziemba, Luke; Thornhill, L. Kenneth; Anderson, Bruce; Diskin, Glenn; Perring, E. Anne; P. Schwarz, Joshua; Campuzano-Jost, Pedro; A. Day, Douglas; B. Palm, Brett; Jimenez, L. Jose; Nenes, Athan, R. J. (2015). Evolution of brown carbon in wildfire plumes. *Geophysical Research Letters*, 42, 4623–4630. https://doi.org/10.1002/2015GL063897

Foster, K., Pokhrel, R., Burkhart, M., & Murphy, S. (2019). A novel approach to calibrating a photoacoustic absorption spectrometer using polydisperse absorbing aerosol. *Atmospheric Measurement Techniques*, *12*(6), 3351–3363. https://doi.org/10.5194/amt-12-3351-2019

Fuller, K. A., & Kreidenweis, S. M. (1999). Effects of mixing on extinction by carbonaceous particles. *Journal of Geophysical Research*, *104*(D13), 15941–15954. https://doi.org/10.1029/1998JD100069

Garofalo, L. A., Pothier, M. A., Levin, E. J. T., Campos, T., Kreidenweis, S. M., & Farmer, D. K. (2019). Emission and Evolution of Submicron Organic Aerosol in Smoke from Wildfires in the Western United States. *ACS Earth and Space Chemistry*, *3*(7), 1237–1247. https://doi.org/10.1021/acsearthspacechem.9b00125

Grieshop, A. P., Logue, J. M., Donahue, N. M., & Robinson, A. L. (2009). Laboratory investigation of photochemical oxidation of organic aerosol from wood fires 1: Measurement and simulation of organic aerosol evolution. *Atmospheric Chemistry and Physics*, *9*(4), 1263–1277. https://doi.org/10.5194/acp-9-1263-2009

Gouw, J. A. De, Middlebrook, A. M., Warneke, C., Goldan, P. D., Kuster, W. C., Roberts, J. M., et al. (2005). Budget of organic carbon in a polluted atmosphere : Results from the New England Air Quality Study in 2002. *Journal of Geophysical Research*, *110*, 1–22. https://doi.org/10.1029/2004JD005623

Healy, R. M., Wang, J. M., Jeong, C. H., Lee, A. K. Y., Willis, M. D., Jaroudi, E., et al. (2015). Light-absorbing properties of ambient black carbon and brown carbon from fossil fuel and biomass burning sources. *Journal of Geophysical Research: Atmospheres*, *120*(13), 6619–6633. https://doi.org/10.1002/2015JD023382

Hecobian, A., Zhang, X., Zheng, M., Frank, N., Edgerton, E. S., & Weber, R. J. (2010). Water-soluble organic aerosol material and the light-absorption characteristics of aqueous extracts measured over the Southeastern United States. *Atmospheric Chemistry and Physics*, *10*(13), 5965–5977. https://doi.org/10.5194/acp-10-5965-2010

Hurteau, M. D., Westerling, A. L., Wiedinmyer, C., & Bryant, B. P. (2014). Projected effects of climate and development on California wildfire emissions through 2100. *Environmental Science and Technology*, *48*(4), 2298–2304. https://doi.org/10.1021/es4050133

Kirchstetter, T. W., Novakov, T., & Hobbs, P. V. (2004). Evidence that the spectral dependence of light absorption by aerosols is affected by organic carbon. *Journal of Geophysical Research D: Atmospheres*, *109*(21), 1–12. https://doi.org/10.1029/2004JD004999

Krasowsky, T. S., McMeeking, G. R., Wang, D., Sioutas, C., & Ban-Weiss, G. A. (2016). Measurements of the impact of atmospheric aging on physical and optical properties of ambient black carbon particles in Los Angeles. *Atmospheric Environment*, *142*, 496–504. https://doi.org/10.1016/j.atmosenv.2016.08.010

Kleinman, L. I., Sedlacek, A. J., Adachi, K., Buseck, P. R., Collier, S., Dubey, M. K., et al. (2020). Rapid evolution of aerosol particles and their optical properties downwind of wildfires in the western US. *Atmospheric Chemistry and Physics*, *20*(21), 13319–13341. https://doi.org/10.5194/acp-20-13319-2020

Lack, D. A., Lovejoy, E. R., Baynard, T., Pettersson, A., & Ravishankara, A. R. (2006). Aerosol Absorption Measurement using Photoacoustic Spectroscopy: Sensitivity, Calibration, and Uncertainty Developments. *Aerosol Science and Technology*, *40*(9), 697–708. https://doi.org/10.1080/02786820600803917

Lack, D. A., & Cappa, C. D. (2010). Impact of brown and clear carbon on light absorption enhancement, single scatter albedo and absorption wavelength dependence of black carbon. *Atmospheric Chemistry and Physics*, 10(9), 4207–4220. https://doi.org/10.5194/acp-10-4207-2010

Lack, D. A., Langridge, J. M., Bahreini, R., Cappa, C. D., Middlebrook, A. M., & Schwarz, J. P. (2012a). Brown carbon and internal mixing in biomass burning particles. *Proceedings of the National Academy of Sciences of the United States of America*, *109*(37), 14802–14807. https://doi.org/10.1073/pnas.1206575109

Lack, D. A., Richardson, M. S., Law, D., Langridge, J. M., Cappa, C. D., McLaughlin, R. J., & Murphy, D. M. (2012b). Aircraft Instrument for Comprehensive Characterization of Aerosol Optical Properties, Part 2: Black and Brown Carbon Absorption and Absorption Enhancement Measured with Photo Acoustic Spectroscopy. *Aerosol Science and Technology*, *46*(5), 555–568. https://doi.org/10.1080/02786826.2011.645955

Lindaas, J., Pollack, I. B., Garofalo, L. A., Pothier, M. A., Farmer, D. K., Kreidenweis, S. M., et al. (2021). Emissions of Reactive Nitrogen From Western U.S. Wildfires During Summer 2018. *Journal of Geophysical Research: Atmospheres*, 126(2), 1–21. https://doi.org/10.1029/2020JD032657

Liu, D., Whitehead, J., Alfarra, M. R., Reyes-villegas, E., Spracklen, D. V, Reddington, C. L., et al. (2017). Black-carbon absorption enhancement in the atmosphere determined by particle mixing state. *Nature Geoscience*, *10*(3), 184–188. https://doi.org/10.1038/NGEO2901

Liu, D., He, C., Schwarz, J. P., & Wang, X. (2020). Lifecycle of light-absorbing carbonaceous aerosols in the atmosphere. *Npj Climate and Atmospheric Science*, *3*(40). https://doi.org/10.1038/s41612-020-00145-8

Liu, J., Bergin, M., Guo, H., King, L., Kotra, N., Edgerton, E., & Weber, R. J. (2013). Size-resolved measurements of brown carbon in water and methanol extracts and estimates of their contribution to ambient fine-particle light absorption. *Atmospheric Chemistry and Physics*, 13(24), 12389–12404. https://doi.org/10.5194/acp-13-12389-2013

Liu, S., Aiken, A. C., Gorkowski, K., Dubey, M. K., Cappa, C. D., Williams, L. R., et al. (2015). Enhanced light absorption by mixed source black and brown carbon particles in UK winter. *Nature Communications*, *6*, 8435. https://doi.org/10.1038/ncomms9435

Marple, V. A., Rubow, K. L., & Behm, S. M. (1991). A microorifice uniform deposit impactor (moudi): Description, calibration, and use. *Aerosol Science and Technology*, *14*(4), 434–436. https://doi.org/10.1080/02786829108959504

McClure, C. D., Lim, C. Y., Hagan, D. H., Kroll, J. H., & Cappa, C. D. (2020). Biomass-burning-derived particles from a wide variety of fuels - Part 1: Properties of primary particles. *Atmospheric Chemistry and Physics*, *20*(3), 1531–1547. https://doi.org/10.5194/acp-20-1531-2020

McConnell, J. R., Edwards, R., Kok, L. G., Flanner, M. G., Zender, C. S., Saltzman, E. S., et al. (2007). 20th-Century Industrial Black Carbon Emissions Altered Arctic Climate Forcing. *Science*, *317*(5843), 1381–1384. https://doi.org/10.1126/science.1144856

Moharreri, A., Craig, L., Dubey, P., Rogers, D. C., & Dhaniyala, S. (2014). Aircraft testing of the new Blunt-body Aerosol Sampler (BASE). *Atmospheric Measurement Techniques*, *7*(9), 3085–3093. https://doi.org/10.5194/amt-7-3085-2014

Neumann, J. E., Amend, M., Anenberg, S., Kinney, P. L., Sarofim, M., Martinich, J., et al. (2021). Estimating PM2.5-related premature mortality and morbidity associated with future wildfire emissions in the western US. *Environmental Research Letters*, 16(3). https://doi.org/10.1088/1748-9326/abe82b

Onasch, T. B., Massoli, P., Kebabian, P. L., Hills, F. B., Bacon, F. W., & Freedman, A. (2015). Single scattering albedo monitor for airborne particulates. *Aerosol Science and Technology*, *49*(4), 267–279. https://doi.org/10.1080/02786826.2015.1022248

Orsini, D. A., Ma, Y., Sullivan, A., Sierau, B., Baumann, K., & Weber, R. J. (2003). Refinements to the particle-into-liquid sampler (PILS) for ground and airborne measurements of water soluble aerosol composition. *Atmospheric Environment*, *37*(9–10), 1243–1259. https://doi.org/10.1016/S1352-2310(02)01015-4

Palm, B. B., Peng, Q., Fredrickson, C. D., Lee, B. H., Garofalo, L. A., Pothier, M. A., et al. (2020). Quantification of organic aerosol and brown carbon evolution in fresh wildfire plumes. *Proceedings of the National Academy of Sciences of the United States of America*, *117*(47), 29469–29477. https://doi.org/10.1073/pnas.2012218117

Peltier, R. E., Weber, R. J., & Sullivan, A. P. (2007). Investigating a liquid-based method for online organic carbon detection in atmospheric particles. *Aerosol Science and Technology*, *41*(12), 1117–1127. https://doi.org/10.1080/02786820701777465

Peng, J., Hu, M., Guo, S., Du, Z., Zheng, J., Shang, D., et al. (2016). Markedly enhanced absorption and direct radiative forcing of black carbon under polluted urban environments. *Proceedings of the National Academy of Sciences of the United States of America*, *113*(16), 4266–4271. https://doi.org/10.1073/pnas.1602310113

Peng, Q., Palm, B. B., Melander, K. E., Lee, B. H., Hall, S. R., Ullmann, K., et al. (2020). HONO Emissions from Western U.S. Wildfires Provide Dominant Radical Source in Fresh Wildfire Smoke. *Environmental Science and Technology*, *54*(10), 5954–5963. https://doi.org/10.1021/acs.est.0c00126

Permar, W., Wang, Q., Selimovic, V., Wielgasz, C., Yokelson, R. J., Hornbrook, R. S., et al. (2021). Emissions of Trace Organic Gases From Western U.S. Wildfires Based on WE-CAN Aircraft Measurements. *Journal of Geophysical Research: Atmospheres*, *126*(11). https://doi.org/10.1029/2020JD033838

Pokhrel, R. P., Wagner, N. L., Langridge, J. M., Lack, D. A., Jayarathne, T., Stone, E. A., et al. (2016). Parameterization of single-scattering albedo (SSA) and absorption Ångström exponent (AAE) with EC/OC for aerosol emissions from biomass burning. *Atmospheric Chemistry and Physics*, *16*(15), 9549–9561. https://doi.org/10.5194/acp-16-9549-2016

Pokhrel, R. P., Beamesderfer, E. R., Wagner, N. L., Langridge, J. M., Lack, D. A., Jayarathne, T., et al. (2017). Relative importance of black carbon, brown carbon, and absorption enhancement from clear coatings in biomass burning emissions. *Atmospheric Chemistry and Physics*, *17*(8), 5063–5078. https://doi.org/10.5194/acp-17-5063-2017

Rosencwaig, A. (1980). *Photoacoustics and photoacoustic spectroscopy*. *Annual Review of Biophysics and Bioengineering*, *9*, 31–54. https://doi.org/10.1146/annurev.bb.09.060180.000335

Saleh, R., Robinson, E. S., Tkacik, D. S., Ahern, A. T., Liu, S., Aiken, A. C., et al. (2014). Brownness of organics in aerosols from biomass burning linked to their black carbon content. *Nature Geoscience*, 7(9), 647–650. https://doi.org/10.1038/ngeo2220

Saleh, R. (2020). From Measurements to Models: Toward Accurate Representation of Brown Carbon in Climate Calculations. *Current Pollution Reports*, *6*(2), 90–104. https://doi.org/10.1007/s40726-020-00139-3

Sarangi, C., Qian, Y., Rittger, K., Leung, R. L., Chand, D., Bormann, K. J., & Painter, T. H. (2020). Dust dominates high-altitude snow darkening and melt over high-mountain Asia. *Nature Climate Change*, (October), 1–7. https://doi.org/10.1038/s41558-020-00909-3

Schnaiter, M., Horvath, H., Möhler, O., Naumann, K. H., Saathoff, H., & Schöck, O. W. (2003). UV-VIS-NIR spectral optical properties of soot and soot-containing aerosols. *Journal of Aerosol Science*, *34*(10), 1421–1444. https://doi.org/10.1016/S0021-8502(03)00361-6

Schnaiter, M., Linke, C., Möhler, O., Naumann, K. H., Saathoff, H., Wagner, R., et al. (2005). Absorption amplification of black carbon internally mixed with secondary organic aerosol. *Journal of Geophysical Research D: Atmospheres*, *110*(19), 1–11. https://doi.org/10.1029/2005JD006046

Schwarz, J. P., Gao, R. S., Fahey, D. W., Thomson, D. S., Watts, L. A., Wilson, J. C., et al. (2006). Single-particle measurements of midlatitude black carbon and light-scattering aerosols from the boundary layer to the lower stratosphere. *Journal of Geophysical Research*, *111*, D16207. https://doi.org/10.1029/2006JD007076

Subramanian, R., Kok, G. L., Baumgardner, D., Clarke, A., Shinozuka, Y., Campos, T. L., et al. (2010). Black carbon over Mexico: The effect of atmospheric transport on mixing state, mass absorption cross-section, and BC/CO ratios. *Atmospheric Chemistry and Physics*, *10*(1), 219–237. https://doi.org/10.5194/acp-10-219-2010

Sullivan, A. P., Pokhrel, R. P., Shen, Y., Murphy, S. M., Toohey, D. W., Campos, T., Lindaas, J., Fischer, E. V., and Collett Jr., J. L. (2022). Examination of Brown Carbon Absorption from Wildfires in the Western U.S. During the WE-CAN Study. *Atmospheric Chemistry and Physics*, *22*(20), 13389–13406. https://doi.org/10.5194/acp-22-13389-2022

Sun, Y., Zhang, Q., Zheng, M., Ding, X., Edgerton, E. S., & Wang, X. (2011). Characterization and source apportionment of water-soluble organic matter in atmospheric fine particles (PM2.5) with high-resolution

aerosol mass spectrometry and GC-MS. *Environmental Science and Technology*, *45*(11), 4854–4861. https://doi.org/10.1021/es200162h

Szopa, S., V. Naik, B. Adhikary, P. Artaxo, T. Berntsen, W.D. Collins, S. et al. (2021): Short-Lived Climate Forcers. In Climate Change 2021: The Physical Science Basis. Contribution of Working Group I to the Sixth Assessment Report of the Intergovernmental Panel on Climate Change. Cambridge University Press, Cambridge, United Kingdom and New York, NY, USA, pp. 817–922, https://doi:10.1017/9781009157896.008

Tasoglou, A., Louvaris, E., Florou, K., Liangou, A., Karnezi, E., Kaltsonoudis, C., et al. (2020). Aerosol light absorption and the role of extremely low volatility organic compounds. *Atmospheric Chemistry and Physics*, *20*(19), 11625–11637. https://doi.org/10.5194/acp-20-11625-2020

Taylor, J. W., Wu, H., Szpek, K., Bower, K., Crawford, I., Flynn, M. J., et al. (2020). Absorption closure in highly aged biomass burning smoke. *Atmospheric Chemistry and Physics*, *20*(19), 11201–11221. https://doi.org/10.5194/acp-20-11201-2020

Wang, X., Sedlacek, A. J., DeSá, S. S., Martin, S. T., Alexander, M. L., Alexander, M. L., et al. (2016). Deriving brown carbon from multiwavelength absorption measurements: Method and application to AERONET and Aethalometer observations. *Atmospheric Chemistry and Physics*, 16(19), 12733–12752. https://doi.org/10.5194/acp-16-12733-2016

Wang, X., Heald, C. L., Liu, J., Weber, R. J., Campuzano-Jost, P., Jimenez, J. L., et al. (2018). Exploring the observational constraints on the simulation of brown carbon. *Atmospheric Chemistry and Physics*, 18(2), 635–653. https://doi.org/10.5194/acp-18-635-2018

Wei, Y., Ma, L., Cao, T., Zhang, Q., Wu, J., Buseck, P. R., & Thompson, J. E. (2013). Light scattering and extinction measurements combined with laser-induced incandescence for the real-time determination of soot mass absorption cross section. *Analytical Chemistry*, *85*(19), 9181–9188. https://doi.org/10.1021/ac401901b

Westerling, A. L., Hidalgo, H. G., Cayan, D. R., & Swetnam, T. W. (2006). Warming and Earlier Spring Increase Western U. S. Forest Wildfire Activity. *Science*, *313*(5789), 940–943. https://doi.org/10.1126/science.1128834

Williams, E. L., & Grosjean, D. (1990). Removal of Atmospheric Oxidants with Annular Denuders. *Environmental Science and Technology*, 24(6), 811–814. https://doi.org/10.1021/es00076a002

Wonaschütz, A., Hitzenberger, R., Bauer, H., Pouresmaeil, P., Klatzer, B., Caseiro, A., & Puxbaum, H. (2009). Application of the integrating sphere method to separate the contributions of brown and black carbon in atmospheric aerosols. *Environmental Science and Technology*, *43*(4), 1141–1146. https://doi.org/10.1021/es8008503

Yue, X., Mickley, L. J., Logan, J. A., & Kaplan, J. O. (2013). Ensemble projections of wildfire activity and carbonaceous aerosol concentrations over the western United States in the mid-21st century. *Atmospheric Environment*, *77*, 767–780. https://doi.org/10.1016/j.atmosenv.2013.06.003

Zeng, L., Zhang, A., Wang, Y., Wagner, N. L., Katich, J. M., Schwarz, J. P., et al. (2020). Global Measurements of Brown Carbon and Estimated Direct Radiative Effects. *Geophysical Research Letters*, 47(13). https://doi.org/10.1029/2020GL088747

Zeng, L., Sullivan, A. P., Washenfelder, R. A., Dibb, J., Scheuer, E., Campos, T. L., et al. (2021). Assessment of online water-soluble brown carbon measuring systems for aircraft sampling. *Atmospheric Measurement Techniques*, *14*(10), 6357–6378. https://doi.org/10.5194/amt-14-6357-2021

Zeng, L., Dibb, J., Scheuer, E., Katich, J. M., Schwarz, J. P., Bourgeois, I., et al. (2022). Characteristics and Evolution of Brown Carbon in Western United States Wildfires. *Atmospheric Chemistry and Physics*, 22, 8009–8036. https://doi.org/10.5194/acp-22-8009-2022

Zhang, L., Segal-Rozenhaimer, M., Che, H., Dang, C., Sedlacek III, A. J., Lewis, E. R., Dobracki, A., Wong, J. P. S., Formenti, P., Howell, S. G., and Nenes, A.: Light Absorption by Brown Carbon over the South-East Atlantic Ocean, *Atmos. Chem. Phys. Discuss*. [preprint], https://doi.org/10.5194/acp-2021-1000, in review, 2022.

Zhang, Y., Forrister, H., Liu, J., DIbb, J., Anderson, B., Schwarz, J. P., et al. (2017). Top-of-atmosphere radiative forcing affected by brown carbon in the upper troposphere. *Nature Geoscience*, *10*(7), 486–489. https://doi.org/10.1038/ngeo2960